Sleep exerts lasting effects on hematopoietic stem cell function and diversity

Cameron S. McAlpine[1,2,3,†,*], Máté G. Kiss[1,3,†], Faris M. Zuraikat[4,8], David Cheek[3], Giulia Schiroli[5,6], Hajera Amatullah[7], Pacific Huynh[1], Mehreen Z. Bhatti[8], Lai-Ping Wong[9], Abi G. Yates[1], Wolfram C. Poller[1,3], John E. Mindur[3], Christopher T. Chan[1,3], Henrike Janssen[1,3], Jeffrey Downey[1,3], Sumnima Singh[1,3], Ruslan I. Sadreyev[9,10], Matthias Nahrendorf[3], Kate L. Jeffrey[7], David T. Scadden[5,6], Kamila Naxerova[3], Marie-Pierre St-Onge[4,8,*], Filip K. Swirski[1,3,*]

Affiliations:
1. Cardiovascular Research Institute and the Department of Medicine, Cardiology, Icahn School of Medicine at Mount Sinai, New York, NY
2. Friedman Brain Institute and the Nash Family Department of Neuroscience, Icahn School of Medicine at Mount Sinai, New York, NY
3. Center for Systems Biology and the Department of Radiology, Massachusetts General Hospital and Harvard Medical School, Boston, MA
4. Sleep Center of Excellence, Department of Medicine, Columbia University Irving Medical Center, New York, NY
5. Center for Regenerative Medicine, Massachusetts General Hospital, Boston, MA
6. Department of Stem Cell and Regenerative Biology, Harvard Stem Cell Institute, Harvard University, Cambridge MA
7. Division of Gastroenterology and Center for the Study of Inflammatory Bowel Disease, Department of Medicine, Massachusetts General Hospital and Harvard Medical School, Boston, MA
8. Division of General Medicine, Department of Medicine, Columbia University Irving Medical Center, New York, NY
9. Department of Molecular Biology, Massachusetts General Hospital and Department of Genetics, Harvard Medical School, Boston, MA
10. Department of Pathology, Massachusetts General Hospital and Harvard Medical School, Boston, MA

†These authors contributed equally to this work

*Corresponding authors:
Cameron S. McAlpine
Cardiovascular Research Institute
Department of Medicine, Cardiology
Nash Family Department of Neuroscience
Icahn School of Medicine at Mount Sinai
One Gustave L. Levy Place, Box 1030
New York, NY, 10029
cameron.mcalpine@mssm.edu

Marie-Pierre St-Onge
Sleep Center of Excellence
Division of General Medicine, Department of Medicine
Columbia University Irving Medical Center
622 West 168th Street, PH9-103H
New York, NY, 10032
ms2554@cumc.columbia.edu

Filip K. Swirski
Cardiovascular Research Institute
Department of Medicine, Cardiology
Icahn School of Medicine at Mount Sinai
One Gustave L. Levy Place, Box 1030
New York, NY, 10029
filip.swirski@mssm.edu

Summary: Sleep interruption restructures the epigenome of hematopoietic stem and progenitor cells (HSPCs) and increases their proliferation, priming them for exaggerated inflammatory bursts and reducing hematopoietic clonal diversity through accelerated genetic drift. In humans, sleep restriction alters the HSPC epigenome and activates hematopoiesis.

Running title: Sleep alters prolonged HSPC function and diversity

Non-standard abbreviations
HSPC: Hematopoietic stem and progenitor cell
CVD: Cardiovascular disease
BM: Bone marrow
SF: Sleep fragmentation
RS: Recovery sleep
SR: Sleep restriction
ZT: Zeitgeber
EEG: Electroencephalography
EMG: electromyography
SWS: Slow wave sleep
REM: Rapid eye movement sleep
LSK: Lineage^{-}Sca1^{+}cKit^{+}
HDAC: histone deacetylase
HAT: histone acetyl transferase
ATAC: assay for transposase-accessible chromatin
CLP: Cecal ligation and puncture
4PBA: 4-phenylbutyrate
BET: bromodomain and extraterminal
CH: clonal hematopoiesis
SDI: Simpson's diversity index
CSF1: Colony stimulating factor 1
IL-3: Interleukin-3

ABSTRACT

A sleepless night may feel awful in its aftermath, but sleep's revitalizing powers are substantial, perpetuating the idea that convalescent sleep is a consequence-free physiological reset. Although recent studies have shown that catch-up sleep insufficiently neutralizes the negative effects of sleep debt, the mechanisms that control prolonged effects of sleep disruption are not understood. Here we show that sleep interruption restructures the epigenome of hematopoietic stem and progenitor cells (HSPCs) and increases their proliferation, thus reducing hematopoietic clonal diversity through accelerated genetic drift. Sleep fragmentation exerts a lasting influence on the HSPC epigenome, skewing commitment towards a myeloid fate, and priming cells for exaggerated inflammatory bursts. Combining hematopoietic clonal tracking with mathematical modeling, we infer that sleep preserves clonal diversity by limiting neutral drift. In humans, sleep restriction alters the HSPC epigenome and activates hematopoiesis. These findings show that sleep slows decay of the hematopoietic system by calibrating the hematopoietic epigenome, constraining inflammatory output, and maintaining clonal diversity.

INTRODUCTION

Sleep profoundly influences immune and inflammatory responses, protecting against age-associated immune disorders including cardiovascular disease (CVD), cancer, and neurodegenerative diseases (Besedovsky, Lange and Haack, 2019; Irwin, 2019). Despite these associations, more than half of adults do not get sufficient sleep (Ford, Cunningham and Croft, 2015; Langer and Filer, 2020). Sleep impacts many facets of the immune system including adaptive responses, inflammation, and the synthesis of cytokines and immune mediators (Dimitrov *et al.*, 2004; Lange *et al.*, 2006; Irwin, 2019). Yet, the influence of sleep on hematopoietic stem and progenitor cells (HSPCs) and immune cell production is poorly understood. In humans, poor quality sleep and sleep disorders associate with increased blood myeloid cells (Ruiz *et al.*, 2012; Geovanini *et al.*, 2018; Vallat *et al.*, 2020) and in murine models sufficient sleep restricts leukocytosis by limiting HSPC cycling in the bone marrow (BM) through neuro-immune mechanisms (McAlpine *et al.*, 2019). In human and murine

atherosclerotic CVD, prolonged sufficient sleep reduces the number of blood monocytes and neutrophils, constraining leukocyte infiltration into the arterial wall and reducing lesion size (McAlpine *et al.*, 2019; Vallat *et al.*, 2020). It has remained unclear, however, how sleep might influence HSPC programming and function.

Sleep abundance and quality vary over an individual's lifespan (Ohayon *et al.*, 2004; Kamel and Gammack, 2006) and the impact of sleep variability on long-term immune related outcomes is unclear. Sleep declines with age (Unruh *et al.*, 2008) and even young healthy adults are prone to vacillations between periods of adequate and insufficient sleep (Lallukka *et al.*, 2012; Ferguson *et al.*, 2021), which can be shaped by genetically-imprinted chronotypes and altered by lifestyle and environments. Bouts of suboptimal sleep, even if followed by periods of sufficient sleep, may have adverse health effects, and recent studies using large human cohorts have indicated that so called "catch-up" sleep is insufficient at reversing or even neutralizing the adverse effects of sleep debt (Depner *et al.*, 2019; Leger *et al.*, 2020; Dashti *et al.*, 2021). Despite these observations, the impact of sleep and oscillations in sleep quality on future immune function and disease susceptibility are poorly understood, yet critical to uncovering the links between sleep and chronic immune and inflammatory diseases that develop over decades. In this study, we explored how sleep fragmentation (SF) and its recovery shape immunological responses and disease outcomes through epigenetic restructuring of HSPCs. We assess the impact of SF on the clonal diversity of immune cells and the genetic aging of the hematopoietic system. To expand our analysis, we quantify hematopoiesis and HSPC programing in humans participating in a sleep restriction trial.

RESULTS

Sleep exerts a prolonged influence on hematopoiesis

To explore how sleep might influence prolonged immune function we first subjected mice to mechanical sleep fragmentation (SF), tactilely rousing mice every 2 minutes during their rest period (Zeitgeber, ZT0-12) (McAlpine *et al.*, 2019). We recorded electroencephalography (EEG) signals from the brain and electromyography (EMG) signals from muscle to quantify sleep and wake states and transitions. As expected, SF increased the number of wake bouts (transitions from sleep to wake states) during the rest period (**Fig. 1A**). SF did not alter slow wave sleep (SWS), rapid eye movement (REM) sleep, or wake time during the light period (**Fig. 1B**). However, SWS was increased, and wake time was reduced during the first two hours of their active period (ZT13 and 14). We next tested whether fragmented sleep is maintained during long exposures to SF and if it reverts after terminating tactile disruption. We subjected mice to 16 weeks of SF followed by 10 weeks of undisturbed sleep (recovery sleep, RS) while continuously monitoring EEG and EMG signals. Wake bouts remained elevated throughout the entire 16 weeks of SF (**Fig. 1C**). During RS, wake bouts were elevated for the first 2 weeks before returning to baseline for the remaining 8 weeks (**Fig. 1C**). Together, these finding suggest a lasting if not permanent influence of SF on sleep quality.

In mice, 16 weeks of SF augments hematopoiesis and the proliferation of Lineage^{-}Sca1^{+}cKit^{+} (LSK) cells in the bone marrow (BM) leading to an increased number of blood Ly6C^{hi} monocytes during the rest period (McAlpine *et al.*, 2019). In the BM, SF increases the concentration of myeloid colony stimulating factor (M-CSF) (McAlpine *et al.*, 2019) but does not alter kit ligand, IL-3, or granulocyte macrophage colony stimulating factor (GM-CSF) (**Fig. S1A-B**). In the plasma, SF raises IL-6 levels while other plasma cytokines, growth factors, corticosterone, and body weight remain unchanged (**Fig. S1C-D**). Considering our data on wake bouts during RS, we sought to determine how long increased leukocyte production persists in mice allowed to recover from 16 weeks of SF. After 4 weeks of RS, at ZT3, blood Ly6C^{hi} monocytes, BM LSKs, and LSK proliferation remained elevated relative to control mice having slept habitually (**Fig. 1D**). However, after 10 weeks of RS in a separate cohort of animals, hematopoietic activity, monocytosis, and IL-6 levels receded to control levels (**Fig. 1 E and Fig S1G**). Relative to control mice, measured plasma and BM cytokines and growth factors, plasma corticosterone, and body weight remained unaltered after 10 weeks of RS (**Fig. S1E-H**). Enhanced hematopoietic activity, therefore, persists for weeks after cessation of SF, raising the possibility that SF exerts a lasting, if not permanent, influence on leukocyte production. To begin to explore this hypothesis, we performed competitive LSK transplantation assays. We transplanted LSKs at a 1:1 ratio from SF (CD45.2) and control (CD45.1) mice into irradiated UBI-GFP mice and allowed recipient mice to sleep habitually. Three weeks after transplantation, we measured the proliferation of LSKs deriving from SF (GFP^{-} CD45.2^{+}) and control (GFP^{-}CD45.1^{+}) animals. Despite similar initial engraftment (**Fig. S1I**) and inhabiting the same BM microenvironment, LSKs of SF mice incorporated more BrdU than controls (**Fig. 1F**). To extend this observation, we tracked CD45.1/2 chimerism in the blood up to 24 weeks post-transplant. Cells arising from SF mice outcompeted cells from control mice and comprised greater than 60% of the leukocyte and monocyte fractions in the blood (**Fig. 1G)**. We made similar observations when LSKs from CD45.2 SF mice were placed

in competition with LSKs from UBI-GFP mice (CD45.2) sleeping habitually (**Fig S1J**). Combined, these findings point to stem-intrinsic mechanisms that regulate prolonged SF-mediated hematopoietic activity.

Sleep programs the epigenome of hematopoietic progenitor cells and instructs adaptability

To test stem-intrinsic mechanisms of sleep-mediated hematopoiesis, we profiled the epigenome of hematopoietic progenitor cells in the BM. First, we observed increased histone deacetylase (HDAC) activity in hematopoietic progenitor cells of SF mice **(Fig. S1K)**. Next, we performed the assay for transposase-accessible chromatin sequencing (ATAC-seq) on LSKs sorted from 3 groups of mice: control mice (habitual sleep), mice subjected to 16 weeks of SF, and mice subjected to 16 weeks of SF followed by 10 weeks of RS (**Fig. 2A**), a time point when LSK number and proliferation have receded (**Fig. 1E**). Though we found ATAC-seq peaks distributed throughout the genome (**Fig. S1L**), we focused our attention on peaks mapping to enhancer elements, which are regions critical to gene expression. Relative to controls, 470 enhancer loci were differentially accessible (DA) in LSKs of SF mice (versus controls, 65 gained accessibility and 405 lost accessibility, Log2FC>2, $p<0.05$, **Fig. 2B and C**), revealing broad reprograming of the epigenome by SF. Next, we compared peaks common to all three groups. We found that 69% (319) of the SF-induced changes in enhancer accessibility reverted to control levels after 10 weeks of RS. However, 31% (140 loci) of alterations caused by SF were maintained in the RS group, representing a preserved signature and a potential mark of sustained epigenetic imprinting (**Fig. 2C**). Pathway analysis of the preserved signature uncovered elements of cell cycle and cell senescence (**Fig. 2D**). These findings reveal that SF restructures the LSK epigenome, and that a cluster of epigenetic imprinting is retained even after prolonged sleep recovery.

The differentiation capacity of hematopoietic progenitor cells is tightly regulated by stem-intrinsic epigenetic modifications to lineage commitment genes (Morrison *et al.*, 1996; Rossi *et al.*, 2005; Dorshkind *et al.*, 2020). We found that SF limited accessibility at enhancers important to lymphocyte lineage differentiation (e.g. *Bcl11a, Ftl3, Sox4, Icos, Il15, Rag1, Pax5, Ets1, Btk*) but augmented accessibility at enhancers associated with myeloid lineage differentiation (*Csf2rb, Irf2bp2, Dyrk3, Erg, Klf9, Klf3, Irfbp2*), suggesting SF restricts lymphoid differentiation and drives LSKs towards a myeloid fate (**Fig. 2E**). Many changes in myeloid enhancers, but not lymphoid enhancers, were retained after 10 weeks of sleep recovery, demonstrating a long-term imprinting of sleep on lineage programming. Enhancers associated with cell cycle regulators (*Cdk11b, Cdk18, Cdkn1b, Cdkn2b*) were also influenced by SF (**Fig. 2E and F**). In agreement with our ATAC-seq findings, transcript expression of the cell cycle inhibitors *Cdkn11b* and *Cdkn2b* was reduced in LSKs of SF mice and remained diminished during recovery, while the cyclin *Cdkal1* and the mediators of lineage fate *Klf9* and *Klf3* were increased in SF mice and remained elevated during recovery (**Fig. 2G**). These analyses suggest that SF skews the hematopoietic system towards the myeloid lineage and the capacity for lymphoid differentiation declines due to stem-intrinsic regulation of lineage commitment genes.

The LSK epigenome instructs secondary recall responses and adaptability (Khan *et al.*, 2020; Divangahi *et al.*, 2021; Rodrigues, Shvedunova and Akhtar, 2021), so we sought to determine whether the preserved epigenetic signature shapes LSKs' response to a subsequent immunological challenge. We allowed mice to either sleep habitually or exposed them to 16 weeks of SF and 10 weeks of RS before subjecting both groups to cecal ligation and puncture (CLP), a model of sepsis and systemic bacteremia (**Fig. 2H**). Twenty-four hours after the CLP, despite equivalent blood bacteremia (**Fig. 2I**), mice exposed to SF followed by RS developed an exaggerated inflammatory response that included heightened blood monocytes and BM LSKs, accelerated LSK proliferation (**Fig. 2I**), and augmented plasma IL-6 and TNFα levels (**Fig. 2J**), but unchanged plasma growth factor and corticosterone levels (**Fig. S1M**). This heightened inflammatory response associated with a worsened clinical score and reduced survival (**Fig. 2K**). To test whether the phenomenon was intrinsic to hematopoietic cells, we transplanted BM cells from control or SF mice into irradiated recipients with no history of sleep disruption (**Fig. 2L**). Ten weeks after the BM transfer, recipients had equivalent blood monocyte counts regardless of whether they received control or SF BM cells (**Fig. 2M**). Recipients were then exposed to CLP and tissues were harvested 24 hours later. Mice that received BM cells from SF mice responded more aggressively to the CLP with increased blood monocytosis (**Fig. 2N**), augmented BM hematopoiesis (**Fig. 2O**) and increased plasma cytokine levels, leading to a worsened clinical score (**Fig. 2P**), indicating these phenotypes are mediated by leukocyte-intrinsic mechanisms. As an alternate re-challenge model, mice subjected to 16 weeks of SF and 10 weeks of RS were re-exposed to SF. Mice experiencing a second bout of SF developed monocytosis and elevated LSK proliferation more rapidly relative to mice experiencing SF for the first time (**Fig. S1N**). Together, these findings suggest that SF creates memory by priming LSKs, leading to augmented inflammatory responses to subsequent immune challenges.

Given our findings, we hypothesized that modifiers of histone acetylation or epigenetic readers might control these lasting effects. To test this hypothesis, we exposed mice to 4-phenylbutyrate (4PBA), a potent HDAC inhibitor, during weeks 8 to 16 of SF. HDAC inhibition did not influence body weight but did blunt SF-induced LSK expansion and the expression of proliferation- and lineage-related genes (**Fig S2**). After habitual sleep or SF, with and without 4PBA treatment, mice underwent RS (while drinking regular water) followed by CLP (**Fig. 3A**). Post-CLP, HDAC inhibition attenuated monocytosis, LSK expansion, LSK proliferation, and plasma cytokines (**Fig. 3B and C**). Similarly, inhibition of bromodomain and extraterminal (BET) reader proteins (Nicodeme *et al.*, 2010) (**Fig. 3D**) restricted the secondary inflammatory response including monocytosis (**Fig. 3E**), BM hematopoiesis (**Fig. 3F**), and plasma cytokine levels (**Fig. 3G**) . These observations support the idea that SF primes LSKs through epigenetic reprograming, rendering adaptability to subsequent inflammatory responses.

Sleep maintains hematopoietic clonal diversity

Having shown that SF has sustained effects on the LSK epigenome, lineage commitment, and turnover, we considered possible implications of these perturbations on somatic evolution of the LSK population. The expansion of hematopoietic clones and the homogenization of the hematopoietic system is a common age-associated pre-malignant condition known as clonal hematopoiesis (CH) (Jaiswal *et al.*, 2014). CH can be driven by accrual of somatic mutations, most commonly in the epigenetic modifiers *Tet2* and *Dmnt3a* (Genovese *et al.*, 2014). CH associates with accelerated epigenetic aging of HSPCs (Nachun *et al.*, 2021), a 2-fold increased clinical risk of cardiovascular disease (Jaiswal *et al.*, 2017), and all-cause mortality (Jaiswal *et al.*, 2014). Recently, we showed that increased HSPC proliferation caused by SF accelerates the emergence of *Tet2*-mutant CH (Heyde *et al.*, 2021). Specifically, in mixed chimeric animals exposed to SF, *Tet2*-mutant cells expand at a faster rate relative to animals whose sleep was unaltered, resulting in mutants encompassing a greater proportion of blood myeloid cells and BM HSPCs (Heyde *et al.*, 2021). However, the majority of CH cases arise in the absence of detectable driver mutations (Zink *et al.*, 2017; Poon *et al.*, 2021; Mitchell *et al.*, 2022). We predicted that heightened proliferation of HSPCs would not only accelerate the expansion of mutant clones but would also expedite neutral evolution – random fluctuations in mutant frequencies due to stochastic loss and self-renewal of HSPCs (Heyde *et al.*, 2021). Even in the absence of mutant selection, diversity declines over time in stochastically self-renewing stem cell populations due to neutral drift (Snippert *et al.*, 2010), an effect that is accelerated under conditions of increased cell turnover. We set out to investigate experimentally our theoretical prediction that drift would be accelerated in mice subjected to SF (Heyde *et al.*, 2021).

We utilized a multi-color LSK clonal-tracking system (Yu *et al.*, 2016; Shen *et al.*, 2021). Briefly, sorted LSKs were stochastically and permanently tagged *ex vivo* with up to 7 fluorophores and transplanted into lethally irradiated recipient mice (**Fig. 4A**). Flow cytometry and a binary gating strategy allowed us to track 127 clusters that incorporated at least one tag and had a unique fluorophore combination (**Fig. 4B**). We evaluated tagged LSK clusters and their descendants, which retain the fluorescent tag of the progenitor cell from which they derive. First, we confirmed that 126 clusters (99%) were detectable among the tagged LSK cells prior to transplantation into recipient mice (**Table S1** and **Fig. S3A**). Six weeks after transplantation, 110±3 clusters (87%) were detectable among blood leukocytes (**Fig. S3B**) with minimal variability between recipient mice (**Fig. S3C**). Cluster frequency of blood monocytes and neutrophils correlated remarkably with cluster frequency of BM LSKs (**Fig. S3D**)**,** demonstrating that changes in cluster abundance and dynamics in the blood are reflective of changes among BM hematopoietic progenitors.

We subjected the recipient mice to habitual sleep or SF and analyzed cluster dynamics in the blood over time. First, we measured the relative change in frequency of clusters with 4 or more tags, which represent rare and more homogeneous clusters (**Table S1**). Among blood monocyte and neutrophil clusters, we found that over time the range of cluster frequencies, the change in mean cluster frequency, and the cluster variance was substantially elevated in SF mice (**Fig. 4C and D**), signifying that SF accelerates the expansion of some clusters and the disappearance of others, consistent with expedited neutral drift. We did not observe changes in relative mean cluster frequency, range, or variance among B and T cell populations, presumably owning to the long half-life of these cells (**Fig. S4A and C**) (Heyde *et al.*, 2021). To directly quantify the evolution of diversity and neutral drift over time, we computed Simpson's diversity index (SDI). We found that in control animals, the SDI of blood monocytes and neutrophils decreased gradually over time (**Fig. 4E and F**). In SF mice however, monocyte and neutrophil SDI decayed more rapidly (**Fig. 4E and F**), consistent with the effects of accelerated neutral drift due to increased cell turnover. We did not observe an influence of SF on

lymphocyte SDI (**Fig. S4B and D**). Together, these data show that SF increases stochastic fluctuations in the frequencies of neutral clusters, thereby reducing hematopoietic cell diversity over time.

Having observed diversity decay through accelerated neutral drift among circulating myeloid cells of SF mice, we turned our attention to progenitors in the BM. Among BM LSKs, 18 weeks of SF increased the mean variance of cluster frequencies and decreased the SDI (**Fig. 4G**), providing direct evidence for accelerated neutral drift and reduced diversity amongst hematopoietic progenitors. To garner insights into the impact of sleep on population diversity as LSKs differentiate into mature cells, we assessed relative changes in SDI of BM LSKs and circulating cells. We found that in both control and SF mice, diversity was higher in BM LSKs than in differentiated blood cells (**Fig. 4H and Fig. S4E**), reflective of the multipotency and unequal contribution of LSKs to circulating immune cells (Pietras *et al.*, 2015). The reduction in SDI between BM LSKs and blood monocytes was greater in SF animals (**Fig. 4H and Fig. S4E**), suggesting that SF limits diversity during monocyte generation. These findings demonstrate that sleep maintains the diversity and restricts the neutral drift of BM hematopoietic stem and progenitor cells by limiting cell turnover.

Next, we tested whether the rate of SF-induced LSK proliferation inferred from our clonal tracking data was quantitatively consistent with independent experimental observations. We mathematically modelled LSK evolution based on the Moran process of population genetics (see methods). For this model, we calculated that the LSK SDI decays at a rate proportional to the rate of cellular proliferation divided by the population size. Using the observed LSK population size after 18 weeks of SF (**Fig. 4I** and **Table S2**), our model estimated a 1.56±0.26-fold increase in LSK proliferation in SF mice. We confirmed this mathematical prediction experimentally by measuring a 1.52-fold increase in BrdU incorporation in LSKs of SF mice (**Fig. 4J**). Using complementary mathematical and experimental methods, our data provide evidence that SF accelerates LSK proliferation and thus neutral drift, rendering the population more homogeneous over time.

Sleep restriction enhances hematopoietic activity and monocytosis in humans

Having established a role for sleep in maintaining the LSK epigenome, immune memory, and clonal diversity in mice, we turned our attention to humans. To test the influence of sleep on hematopoiesis and the epigenome of human hematopoietic progenitor cells, we collected blood samples from humans participating in a randomized crossover study in a free-living setting in which chronic mild insufficient sleep was imposed on healthy young volunteers (mean age 35.7±15.1 years) with adequate habitual sleep duration and free of sleep disorders (**Fig. 5A**, study flow chart in **Fig. S5A**, cohort characteristics in **Table S3**). The study was comprised of a 6-week habitual sleep (HS) phase where participants slept an average of 7.4±0.1 hours per night and a 6-week sleep restriction (SR) phase where participants restricted their sleep to 6.1±0.1 hours per night **(Fig. 5B)**. Participants underwent both study phases, in a random order, which were separated by a washout period of at least 6 weeks. As participants completed each phase, we collected blood in the morning (mean clock time 10:54±0:16) and evening (mean clock time 15:21±0:12), and we analyzed circulating leukocyte populations by flow cytometry. As expected, we detected a circadian pattern characterized by high circulating leukocyte numbers in the evening and low numbers in the morning (**Fig. 5C**). However, we found that after completing SR, participants had more circulating $CD14^{+}CD16^{-}$ classical monocytes and $CD14^{-}CD16^{+}$ non-classical monocytes in the evening, but not morning (**Fig. 5C**). SR did not change intermediate monocytes or B and T cell populations (**Fig. 5C**) and changes in blood monocytes did not depend on energy intake or adiposity (**Fig S5B**). Consistent with our murine findings, these data reveal that sleep protects against blood monocytosis in humans, a phenomenon observable in both species at the start of the resting period (McAlpine *et al.*, 2019).

To build on these observations, we sought to determine whether sleep affects HSPCs in humans. Human $lineage^{-}CD34+$ HSPC numbers fluctuated in the blood according to a circadian rhythm (**Fig. 5D**). We found that SR increased HSPC number in the blood in the evening (**Fig. 5D**), suggesting that, like in the mouse, SR enhances hematopoietic activity in humans. The impact of SR on HSPCs did not depend on energy intake or adiposity (**Fig. S5C**). Next, we investigated whether SR influences the epigenome of human HSPCs. We measured histone acetyl transferase (HAT) and HDAC activity in sorted HSPCs retrieved in the evening and found that SR tended to increase HAT activity and significantly augmented HDAC activity (**Fig. 5E**), which reduced histone H3 acetylation (**Fig. 5F**) and indicated that sleep shapes the epigenome of human HSPCs. As HSPCs differentiate to myeloid cells, they rely on the growth factors CSF1 and IL-3 (Mindur and Swirski, 2019), which signal via CD115 and CD123 respectively. Accordingly, we found enhanced expression of CD115 and CD123 on HSPCs retrieved from participants experiencing SR (**Fig. 5G**). These findings reveal that human sleep mediates hematopoiesis, shapes the HSPC epigenome, and promotes myeloid differentiation cues.

DISCUSSION

Sleep profoundly influences the immune system and its functioning (Besedovsky, Lange and Haack, 2019; Irwin, 2019). However, sleep's impact on hematopoiesis and the programming and clonality of HSPCs have remained unclear. Here, we report that murine SF augments sleep-wake transitions, increases hematopoiesis, and alters the epigenome of HSPCs through changes in histone acetylation. While hematopoiesis recedes during sleep recovery, HSPCs retain epigenetic imprinting, priming them for myeloid-biased responses and increased inflammatory activation during subsequent immune challenge. Using a multicolor clonal-tracking system, we find that SF reduces the diversity of the hematopoietic system by accelerating neutral drift and the emergence and disappearance of HSPC clones. In humans, we show that 6 weeks of mild sleep restriction increases the number of HSPCs and monocytes in the blood, reduces HSPC histone acetylation, and promotes HSPC myeloid response cues. Together, these findings suggest that oscillations in sleep quality and abundance compromise HSPC epigenetic structure, diversity, and subsequent immune function.

Chronic sleep disruption is pervasive in modern lifestyles (Ford, Cunningham and Croft, 2015). Sleep disruption encompasses many permutations including, but not limited to, fragmentation, restriction, social jet lag, obstructive sleep apnea (OSA), and insomnia, which substantially increase susceptibility to immune-associated diseases (Irwin, 2019). Individuals typically do not experience one continuous form of sleep disruption but oscillate between types of sleep disturbance and between periods of inadequate sleep and healthy sleep. To understand the mechanistic links between sleep on chronic age-associated diseases that develop over decades, fluctuations in sleep patterns must be considered. One mechanism by which even short periods of poor sleep might impact future disease pathology is through epigenetic programming. Insufficient sleep, sleep disorders, and shift work markedly alter a cell's epigenome. For example, OSA modifies the epigenome in the cardiovascular system and circulating leukocytes (Chen *et al.*, 2019), and one sleepless night changes DNA methylation in liver and muscle tissue at the transcription start sites of genes associated with metabolism (Cedernaes *et al.*, 2018). Moreover, sleep disorders, including OSA, insomnia, and sleep disordered breathing, alter DNA methylation and accelerate the epigenetic age of blood leukocytes (Carroll *et al.*, 2017; Li *et al.*, 2019). Together, these data suggest that sleep modifies the epigenome of diverse cell types throughout the body. However, it has remained unclear whether these sleep-mediated epigenetic modifications have a subsequent consequence on future cell function, inflammation, and disease pathology. Moreover, the influence of sleep on the epigenetic status of HSPCs was unknown. We provide evidence for sustained epigenetic imprinting of HSPCs by sleep disruption. Our data show that SF-induced epigenetic programing is partially maintained during prolonged convalescent sleep and predisposes the hematopoietic system to overt inflammatory responses to subsequent immune challenges. The preserved epigenetic signature is not sufficient for sustained LSK proliferation and differentiation during sleep recovery, likely owing to the vast genomic program and alternate epigenetic modifications, like methylation, involved in controlling cellular proliferation. These data have important implications to inflammatory diseases such as sepsis, CVD, and cancer, and may suggest that early life sleep behavior dictates future disease severity. Our findings support the hypothesis that periods of poor sleep, even if followed by sleep recovery, have sustained consequences on immunological health.

The systemic networks that connect sleep with HSPC epigenetic rewiring and adaptability require further study. Neural circuits together with neuropeptidergic, neuroendocrine, and inflammatory pathways are likely involved. For example, hypothalamic hypocretinergic signaling controls sleep-mediated HSPC proliferation (McAlpine *et al.*, 2019) and our data suggest that SF raises, while sleep recovery normalizes, systemic IL-6 levels. IL-6 signaling has broad functionality in health and disease (Libby and Rocha, 2018; Ridker and Rane, 2021), and has been linked to sleep and its disruption (Friedman *et al.*, 2005; Hong *et al.*, 2005; Dimitrov *et al.*, 2006), and histone modifications (Samanta *et al.*, 2008). How IL-6 or other immune signaling factors might fit within the sleep–hematopoiesis–epigenome interaction and mediate adaptability after sleep recovery should be explored in detail.

The HSPC epigenome dictates fate, division, and clonality, and mediates age-associated changes to the hematopoietic system (Morrison *et al.*, 1996; Buisman and de Haan, 2019; Rodrigues, Shvedunova and Akhtar, 2021). Clonally expanded HSPCs often harbor mutations in epigenetic modifiers and CH is strongly associated with epigenetic age acceleration (Genovese *et al.*, 2014; Nachun *et al.*, 2021). Therefore, we hypothesized that epigenetic reprogramming and increased proliferation of HSPCs promoted by sleep disruption may influence their clonality and the neutral evolution of the hematopoietic system. Our prior mathematical framework suggested that the magnitude of HSPC clonal expansion is dependent on their proliferative rate and less on their mutations or conferred fitness advantage (Heyde *et al.*, 2021). For example, increased hematopoiesis induced by SF or high-fat-diet feeding accelerates the emergence and clonal

expansion of *Tet2*-mutant HSPCs (Heyde *et al.*, 2021). The theory predicted that a stochastic elevation in hematopoiesis would accelerate neutral drift and the emergence of clones even in the absence of mutant selection. Here, we used a fluorescent tagging system to test this theory experimentally. We find that increased proliferation of mutant-free HSPCs caused by SF accelerates neutral drift, which leads to faster expansion and disappearance of HSPC clones, thus limiting hematopoietic diversity. Our observations support the notion of reverse causality – increased HSPC proliferation accelerates the expansion of mutant and neutral clones. These data add to our understanding of the relationship between CH and inflammatory disorders such as CVD whose risk factors, including sleep disruption, augment hematopoiesis and expedite the emergence of mutant and non-mutant HSPC clones, increasing disease susceptibility.

Humans experiencing sleep fragmentation (Vallat *et al.*, 2020) and OSA (Geovanini *et al.*, 2018) develop blood monocytosis and neutrophilia. However, the influence of sleep on hematopoiesis, HSPC function, and circadian dynamics in humans had not been explored. We found that 6 weeks of chronic mild sleep restriction increased the number of blood monocytes and HSPCs in human subjects but did not influence lymphocyte populations. Whether the elevation in blood HSPCs is due to increased hematopoietic activation through augmented HSPC cycling in the BM and/or increased HSPC release from the BM will require further study. Importantly, these findings were observed in the evening, mirroring our murine data (McAlpine *et al.*, 2019) and suggesting that the time of blood collection is a critical variable when assessing changes in blood leukocyte number. Additionally, our findings reveal that sleep restriction alters the intrinsic epigenome of human HSPCs by reducing histone acetylation through increased HDAC activity. Together, our murine and human data propose that different forms of sleep interruption in species with dissimilar sleep architecture perpetuate similar outcomes on hematopoiesis and monocytosis, underscoring the preserved nature of this phenomenon.

Understanding the prolonged influence of sleep on immune function and disease susceptibility is important, particularly given the nearly pandemic prevalence of insufficient sleep (Watson *et al.*, 2015). Our study provides evidence, in mice and humans, that sleep exerts a lasting influence on the immunity and functioning of HSPCs via epigenetic modification and that sleep fragmentation genetically ages the hematopoietic system by accelerating neutral drift, which collapses clonal diversity and homogenizes the myeloid pool.

MATERIALS AND METHODS

Animal studies

Wild-type C57BL/6J, B6.SJL-Ptprca Pepcb/BoyJ (CD45.1), and C57BL/6-Tg(UBC-GFP)30Scha/J (ubiGFP) mice were purchased from the Jackson Laboratory. Age- and sex- matched mice were used. Where appropriate, mice were randomly assigned to interventions. All mice were group-housed with free access to food and water. All animal protocols were approved by the Animal Review Committee at the Massachusetts General Hospital (protocol nos. 2011N000035 and 2015N000044) or the Icahn School of Medicine at Mount Sinai (Protocol nos. PROTO202100023 and PROTO202000262) and were in compliance with relevant ethical regulations.

In Vivo Interventions

Sleep fragmentation and recovery sleep. For sleep fragmentation studies were performed as previously described (McAlpine *et al.*, 2019). Briefly, mice were placed in a sleep fragmentation chamber (Lafayette Instrument) and the sweep bar moved along the bottom of the cage every 2 min during the light cycle (ZT0–12). The sweep bar automatically shut off and was stationary during the dark cycle (ZT12–24). Control mice whose sleep was unaltered were placed in sleep fragmentation chambers with stationary sweep bars. For recovery experiments the sweep bar was shut off and animals were transferred to a conventional mouse cage.

Telemetry EEG and EMG monitoring. First, animals were implanted with EEG/EMG transmitters (HDx-02, Data Science International). Briefly, the head of the animal was secured in a stereotactic frame and a 2-3cm incision was made along the dorsal midline posterior margin of the eyes to midway between the scapulae. A subcutaneous pocket was formed and the implant was inserted with the biopotential leads oriented cranially. The EMG electrodes were inserted into the cervical trapezius muscle in the dorsal region of the neck and the ends were sutured so they remain in place. To place the EEG electrodes a micro drill was used to perforate the skull above the cortex. The ends of the leads were placed in the hole such that they make contact with the dura of the cortex. The leads were secured in place using dental acrylic. The skin incision was sutured and

mice received post-surgical analgesia and were supplemented with warmth for 1 hour. Mice were allowed to recover for 1 week before monitoring began. Mice were placed in sleep fragmentation or control chambers and EEG/EMG data was recorded using the Data Science International telemetry system and hardware. Ponemah software (DSI) was used to acquire the data and Neuroscore 3 (DSI) was used to perform sleep analysis using standard settings.

Bone marrow transplantation. For competitive transplantation assays, mice were lethally irradiated (950 cGy) and reconstituted with 50,000 LSKs from each donor along with 2,000,000 BM feeder cells (of the same genotype as the recipient mouse) injected intravenously 18 hours after irradiation.

Cecal ligation and puncture (CLP). The CLP procedure was carried out as previously described (Weber *et al.*, 2015). Briefly, the peritoneal cavity was opened during isoflurane anesthesia, and the cecum was exteriorized and ligated at the second arterial vessel or third arterial vessel (for survival studies) distal to the end of the cecum. The ligated portion of the cecum was the perforated using a 17 G needle and a small drop of cecal content was extruded though the puncture. The cecum was relocated into the peritoneal cavity and the peritoneum was closed. Animals were given 1mL of saline and removed from isoflurane.

Reagent administration. 4-phenylbutyrate (4PBA) was dissolved in water at a concentration of 5.75g/L which results in a delivery of ~1.5g/kg/day when given as drinking water. 4PBA-containing drinking water was given to mice at week 8 of SF, removed at week 16, and changed weekly. iBet was dissolved in 20%beta-cyclodextrin and 11% DMSO and intravenously injected into animals at a concentration of 30mg/kg 4 times over 2 days prior to the CLP.

Cells

Collection. Peripheral blood was collected at ZT3 by retro-orbital bleeding and red blood cells were lysed in RBC lysis buffer (Biolegend). Bone marrow cells were collected at ZT3 by flushing bones with PBS, after which a single-cell suspension was created by passing cells through a 26-gauge needle and red blood cells were lysed with RBC lysis buffer. Total viable cell numbers were counted using trypan blue (Cellgro, Mediatech) or counting beads (Thermo Fisher Scientific).

Flow cytometry. Single-cell suspensions were stained in PBS supplemented with 2% FBS and 0.5% BSA. The following monoclonal antibodies were used for flow cytometry analyses: anti-CD45 (BioLegend, clone30-F11, 103147), anti-CD45.1 (BioLegend, clone A20, 110708), anti-CD45.2 (BioLegend, clone 104, 109802), anti-CD3 (BioLegend, clone 17A2, 100206), anti-CD90.2 (BioLegend, clone 53-2.1, 105308), anti-CD19 (BioLegend, clone 6D5, 115508), anti-B220 (BD Biosciences, clone RA3-6B2, 553089), anti-NK1.1 (BioLegend, clone PK136), anti-Ly-6G (BioLegend, clone 1A8, 127614), anti-Ly-6C (BioLegend, AL-21, 128006), anti-CD11b (BioLegend, clone M1/70, 101226), anti-CD115 (BioLegend, clone AFS98, 135517), anti-Ter119 (BioLegend, clone TER-119, 116208), anti-CD34 (eBioscience, clone RAM34, 11-0341-85), anti-CD49b (BioLegend, clone DX5, 1089008), anti-CD11c (BioLegend, clone N418, 117310), anti-IL-7Rα (BioLegend, clone SB/199, 121112), anti-CD16/32 (BioLegend, clone 93, 101324), anti-cKit (BioLegend, clone 2B8, 105814), anti- Sca1 (BioLegend, clone D7, 108126), anti-CD8 (BD Bioscience, clone 53-6.7, 553035), anti-CD4 (BioLegend, clone GK1.5, 100428), anti-BrdU (eBioscience, clone BU20A, 17-5071-42). All antibodies were used in a 1:700 dilution. Viable cells were identified as unstained with 7AAD (BioLegend). Cells were identified as Ly-6Chigh monocytes (CD45+CD11b+CD115+Ly- 6Chigh), neutrophils (CD45+CD11b+Ly-6G+), LSK cells (CD45+Lin−Kit+ Sca1+), B cells (CD45+B220+CD19+CD11b−), T cells (CD45+CD3+CD90+CD8+CD11b−). Lineage was B220, CD19, CD49b, Ter119, CD90.2, CD11b, CD11c, Ly-6G, IL-7Rα. Viable cells were identified as unstained with 7AAD (Biolegend). Data were acquired on a LSRII and a FACS Aria II (BD Biosciences) and analyzed with FlowJo (Tree Star).

BrdU incorporation. To assess cell proliferation, 1 mg BrdU was injected intraperitoneally 2 hours before euthanasia. A BrdU flow kit (BD Biosciences) was used to stain BrdU+ cells.

Cell Sorting. Bone marrow cell suspensions were stained to identify the indicated cell populations and cells were sorted on a FACS Aria II cell sorter (BD Biosciences) directly into collection medium.

Molecular analysis

Quantitative PCR. Total RNA was isolated using the RNeasy Mini Kit (Qiagen) or the NucleoSpin RNA XS kit (Takara Bio) according to the manufacturer's instructions. RNase-free DNase Set (Qiagen) was used for DNase digestion during RNA purification. RNA quantity and quality were assessed by Nanodrop for RNA isolated from tissues and with the Aglient RNA 6000 Pico kit (Aglient Technologies) on the Aglient 2100 Bioanalyzer for RNA of fluorescence-activated cell sorting (FACS)-purified cells. cDNA was generated from 1 µg of total RNA per sample using the High-Capacity cDNA Reverse Transcription Kit (Applied Biosystems). Quantitative real-time TaqMan PCR was performed using the following TaqMan primers (Applied Biosystems): Mm00438168, Mm00483241, Mm00492956, Mm00495172, Mm00507441.

Enzyme-linked immunosorbent assay*.* IL-6, TNFα, IL-1β, M-CSF, and G-CSF levels were measured using an ELISA (Booster Biologics) using manufacturer's instructions. On sorted cells, HAT and HDAC activity were measured using commercially available kits according to manufacturer's instructions. HAT kit (Sigma Aldrich, cat#EPI001), HDAC Kit (Sigma Aldrich, cat#CS1010). Corticosterone was measured using an ELISA (Abcam) and manufacturer's instructions.

ATAC-seq. ATAC-seq was conducted in technical and biological duplicates. Briefly, 20,000 sorted LSK cells were initially resuspended in lysis buffer and centrifuged. The nuclei pellets were then subjected to transposition reaction using the Nextera Tn5 transposase enzyme (Illumina). Tagmented DNA was purified with the MinElute PCR Purification kit and eluted in 10 µl of elution buffer (Qiagen). Barcoded libraries were prepared, and PCR amplified. Double-sided bead purification was performed using AMPure XP beads to remove primer dimers and large >1,000-bp fragments. Libraries were sequenced as 50-bp paired-end reads on an Illumina HiSeq 2500.

Sequencing reads were first mapped to the mm10 reference genome using BWA-MEM66 with default parameters, followed by calling peaks using HOTSPOT2. We identified 41000 peaks, which showed high consistency between biological duplicates. Peaks with differential accessibility between conditions were identified using edgeR68, with cutoffs of at least a Log2Fold change>1.2 difference in normalized read density and $P < 0.05$.

Pathway Analysis. KEGG pathway analysis was done using Enrichr (https://maayanlab.cloud/Enrichr/) with default parameters.

Clinical Scoring

Clinical scoring was performed as previously described (Weber *et al.*, 2015). The clinical score of each animal was assessed as follows (points). [a] appearance: normal (0), lack of grooming (1), piloerection (2), hunched up (3), above and eyes half closed (4); [b] behavior - unprovoked: normal (0), minor changes (1), less mobile and isolated (2), restless or very still (3); behavior - provoked: responsive and alert (0), unresponsive and not alert (3); [c] clinical signs: normal respiratory rate (0), slight changes (1), decreased rate with abdominal breathing (2), marked abdominal breathing and cyanosis (3); [d] hydration status: normal (0), dehydrated (5). The higher the score the worse the clinical situation of the animal.

Survival analysis

Cecal ligation and puncture was performed as described above. Animals were then monitored until they reached endpoint.

Bacterial cultures

Whole blood was diluted in PBS, plated on trypticase soy agar with 5% horse blood, and incubated at 37°C. The number of bacterial colonies was assessed 12-16 hours later.

Generation of fluorescent tagged mice and tracking of clusters.

Donor WT mice were sacrificed and 1,000,000 BM LSKs were sorted and pooled. LSKs were cultured in serum-free StemSpan medium (StemCell Technologies) containing penicillin, streptomycin, glutamine and a combination of cytokines (20 ng/ml IL-3, 100 ng/ml SCF, 100 ng/ml Flt-3L, 50 ng/ml TPO all from Peprotech), at a concentration of 106 cells/ml. After one hour of pre-stimulation, cells were transduced with a mix of highly concentrated lentiviral vectors encoding for different fluorescent proteins (BFP, Sapphire, Venus, KO, mCherry, iRFP, Keima) at a dose of 20 transducing units /cell. After tagging, a small aliquot of cells was analyzed by flow cytometry prior to their transplantation (BM baseline). Recipient mice were lethally irradiated (9.5Gy) and each

were i.v. injected with 100,000 tagged LSKs along with 2,000,000 $Sca1^-$ unlabeled feeder cells. Mice were allowed to recover and sleep habitually for 6 weeks. After recovery, mice were bled and circulating leukocytes were analyzed (blood baseline). Mice were then randomly assigned to SF or habitual sleep. Animals were bled periodically and sacrificed after 18 weeks of SF.

Mathematical calculations of variance. Cells that fluoresced above background were considered positive for an incorporated fluorescent tag. Distinguishing dichotomous populations (positive or negative for a fluorophore) allowed the identification of 127 uniquely tagged clusters plus one cluster that did not incorporate any fluorophores and was excluded from analysis. Fold change in relative frequencies was calculated by dividing cluster frequency by the baseline frequency. Variance (s^2) of cluster frequency was calculated using:

$$s^2 = \frac{\sum_{i=1}^{n}(x_i - \overline{x})^2}{n-1}$$

Where $\overline{x}$ is the mean frequency and n is the number of clusters.

Mathematical calculations of Simpson's diversity and cell division rate estimation. For a single mouse, Simpson's diversity index at time *t* is defined by:

$$D_t = 1 - \sum_{i=1}^{127}(X_{i,t})^2,$$

where $i = 1, .., 127$ denote the tagged clusters and $X_{i,t}$ is the frequency of cluster i at time *t*. To predict the evolution of Simpson's diversity, we model that LSK's divide and die according to the Moran process (Ewens, 2004) which is parameterised by the number of cells *N* and the per cell division rate a. From the Kolmogorov equations (Durrett, 2012), the expected Simpson's diversity follows the differential equation

$$\frac{d}{dt}\mathbb{E}D_t = -\frac{2a}{N}\mathbb{E}D_t,$$

Which has solution

$$\mathbb{E}D_t = D_0 e^{-\frac{2a}{N}t}. \quad (1)$$

It follows that

$$\frac{N_S \log\left(\frac{1}{\#S}\sum_{m\in S}\frac{D_{t,m}}{D_{0,m}}\right)}{N_C \log\left(\frac{1}{\#C}\sum_{m\in C}\frac{D_{t,m}}{D_{0,m}}\right)} \quad (2)$$

is a consistent estimator for a_S/a_C, where *S* is the set of mice in the SF group, *C* is the set of mice in the control group, $D_{t,m}$ is Simpson's diversity at time *t* for mouse *m*, and a_S, a_C , N_S, N_C are the division rates and LSK numbers for the sleep fragmentation and control mice. While control vs SF mice are expected to have similar LSK numbers at the beginning of the experiment, we measure that LSK numbers are 1.4 fold higher in SF vs control mice at 18 weeks. Averaging over the two timepoints, we take $N_S/N_C = 1.2 \pm 0.2$. Plugging this into (2) along with the LSK diversity measurements, an estimate of $a_S/a_C = 1.56 \pm 0.26$ is obtained. That is, LSK's divide at a rate 1.56±0.26 fold faster in SF vs control mice, which is consistent with the BrdU estimate of 1.52.

There are caveats to our division rate estimation. For one, the model of LSK evolution is simplistic. A more detailed model could, for example, consider that division rates and LSK numbers may vary over time and between mice in a group. Moreover, there would ideally be more data points to enable improved estimate precision. Nevertheless, the purpose of the modelling is conceptual. We demonstrate that accelerated genetic drift due to increased division rates can explain sleep fragmentation's impact on LSK diversity.

Human Study

***Study Design*.** The human subjects component of this study employed a randomized crossover design to assess the impact of a common model of chronic insufficient sleep on hematopoiesis in 14 participants. This outpatient trial included 2 sleep conditions: maintenance of habitual adequate sleep (HS) and prolonged mild sleep restriction (SR). Each condition was 6 weeks in duration. The order of conditions was randomized across participants, and study phases were separated by a minimum 6-week washout. In the fifth and sixth weeks of each study condition, blood samples were collected in the late afternoon/early evening (hereafter referred to as early evening) and the morning, respectively, for assessment of hematopoietic outcomes. This investigation was a component of an ongoing clinical trial designed to test the impact of prolonged insufficient sleep on energy balance. The trial was prospectively registered on ClinicalTrials.gov (NCT02960776). All procedures were conducted in accordance with the Declaration of Helsinki and approved by the Columbia University Institutional Review Board (protocol number AAAQ7746); all participants provided informed consent prior to participation.

***Subjects*.** Metabolically-healthy men and women, aged 20-75 y, who were not overweight or obesity, nor at risk for obesity, and with a habitual sleep duration of ≥7 h/night, were recruited through advertisements placed online and throughout the New York City area. Individuals meeting initial eligibility criteria based on a phone interview were invited to the laboratory for an in-person screening visit. During this visit, height and weight were measured in duplicate using calibrated research-grade stadiometer and scale (Tanita WB-3000, Tokyo, Japan), respectively. Body mass index (BMI) was calculated as weight (kg) divided by height (m) squared. Individuals then completed questionnaires validated for assessment of sleep and circadian rhythms as well as a detailed health history questionnaire. Men and women were deemed potentially eligible if they had overweight or class I obesity (BMI 25.0 – 34.9 kg/m^2) or were at risk for obesity (BMI 20.0 – 24.9 kg/m^2 with ≥ 1 parent with BMI > 27 kg/m^2), had good habitual sleep quality (score ≤ 5 on the Pittsburgh Sleep Quality Index (Buysse *et al.*, 1989)), were at low risk for sleep apnea (< 2 positive categories on Berlin Questionnaire (Netzer *et al.*, 1999)), and did not report excessive daytime sleepiness (scores < 10 on the Epworth Sleepiness Scale (Johns, 1991)). Those with extreme morning or evening chronotypes (scores ≤ 30, ≥ 70 on the Morningness-Eveningness Questionnaire (Horne and Ostberg, 1976)), participating in shift work or daytime napping, or had recent travel across time zones (≤ 3 weeks) were not eligible to participate. Exclusion criteria also included current smoking, dieting, recent weight change > 2.5 kg, excessive caffeine intake (> 300 mg/day), use of hormonal contraceptives, pregnant or ≤ 1 y post-partum, as well as presence of cardiovascular, metabolic, neurological, or psychiatric diseases or disorders (including eating and substance abuse disorders). Individuals meeting all eligibility criteria were invited to complete an intensive outpatient sleep screening to ensure habitual adequate sleep duration. Sleep was assessed continuously over 2 consecutive weeks using the Actigraph GT3X + (Actigraph Corporation, Pensacola, FL) and nightly sleep diaries. The Actigraph GT3X+ is a tri-axial accelerometer worn on the non-dominant wrist and validated against polysomnography(Full *et al.*, 2018), the gold standard objective measurement of sleep. Inclusion in the study required a 14-night average total sleep time (TST) of 7-9 h/night with ≥ 7 h of sleep on ≥ 10 of the nights and no more than 3 nights with < 6 h of sleep. To date, 42 participants met these criteria and have been randomly assigned an order of study conditions. Of the full sample, 16 participants (9 women) were accrued for this ancillary study, which began after initiation of the main study; however, 2 individuals dropped out of the study. Thus, the analytic sample was 14 (n=7 women).

Intervention. Participants were studied in a free-living setting over 2 phases of 6 weeks each, differing only in sleep duration condition: HS and SR. In both conditions, habitual patterns of sleep, determined from screening, were used to create fixed personalized sleep schedules in both conditions. In the HS condition, participants were to maintain their average bed and waketimes from screening to achieve their habitual adequate sleep duration of ≥ 7 h/night. In contrast, during SR, participants were instructed to delay their bedtimes (from screening averages), while maintaining habitual wake times, to achieve a reduction in TST of ~90 min/night. In order to promote fidelity to the protocol, bed and wake times were adjusted slightly to the participants' preference. In addition, sleep was monitored continuously using wrist-actigraphy and nightly sleep diaries, and verified weekly by trained study staff, throughout the 6-week study phases to assess compliance. Study phases were separated by a 6-week washout period; sleep was reassessed over the final 2 weeks of this washout period to confirm that participants were achieving average TST ≥ 7 h/night before beginning the next study phase.

Procedures. During each study phase, participants came to the laboratory for a baseline visit (week 0), during which time they completed a number of procedures and received their sleep assignment. Participants returned on a weekly basis for review of wrist-actigraphy data and sleep logs and for additional assessments. Many of these procedures are beyond the scope of this paper. At baseline (week 0) and endpoint visits (week 6), participants underwent MRI scans and peripheral blood was drawn from a vein within the antecubital fossa into an EDTA tube by a trained phlebotomist while participants were in the fasted state. Blood draws at baseline and endpoint visits (week 6) were scheduled for mornings between 09:00 and 11:00. At a separate visit, 5 weeks into each condition, whole blood was collected in the evening (15:00-17:00). The amount of blood collected and time of draw was recorded at all visits and the vast majority of draws (86%) occurred within 1 h of the planned ranges of draw times. Although there was variability in draw times across participants and visits, only one participant had both a late morning draw and an early evening draw during the same phase.

Blood samples were processed shortly after collection for extraction and preservation of viability of blood cells. Whole blood was transferred to a 50 mL conical tube (Corning, Corning, NY) and phosphate-buffer saline (PBS) diluted to 1X (Thermo Fisher Scientific, Waltham, MA) was added to the blood to a final volume of 35 mL. The solution was then carefully underlaid with 15 mL of ficoll-paque PLUS (GE Healthcare, Chicago, IL) and spun for 30 min at 23°C and 1800 RPM with the centrifuge brake off (Eppendorf 5810R, Eppendorf, Hamburg, Germany). The resulting white blood cell layer was aspirated and transferred to a new conical tube; PBS was added to a final volume of 50 mL and then spun for 10 min at 4°C (1800 RPM, brake on). After spinning, the white blood cell pellet was resuspended in freezing media (20% FBS RPMI 1640 [Thermo Fisher Scientific] with 10% DMSO [Sigma Life Sciences]) and transferred into separate 1.5 mL cryovials. The cryovials were frozen at a controlled rate of -1°C/min (Mr. Frosty, Thermo Fisher Scientific) in order to maintain viability of cells and were then transferred to liquid nitrogen for storage until flow cytometry analysis. Neutrophils are not included in the leukocytes isolated by ficoll-plaque PLUS gradient as they are pelleted and discarded.

Human flow cytometry. For flow cytometry of human leukocytes, cells were quickly warmed in a 37°C water bath. 1mL of prewarmed RPMI1640 media containing 10% FBS was added to the cells. Cells were transferred to a 15mL tube containing 10mL of 10% FBS RPMI1640 media. Cells were spun at 200g for 10 mins and washed in PBS before staining with antibodies. Cells were stained in PBS supplemented with 2% FBS, 0.5% BSA, and 0.5% EDTA. The following monoclonal antibodies (clone) were used at a dilution of 1/700 unless otherwise indicated: anti-CD2 (RPA-2.10), anti-CD3 (HIT3a), anti-CD4 (RPA-T4), anti-CD8 (RPA-T8), anti-CD10 (HI10a), anti-CD11b (ICRF44), anti-CD14 (HCD14), anti-CD16 (3G8), anti-CD19 (H1B19), anti-CD20 (3H7), anti-CD56 (HCD56), anti-CD235 (HI264), anti-CD90 (2E10), anti-CD115 (9-4D2-1E4), anti-CD123 (6H6), anti-CD34 (8G12), anti-IgD (IA6-2), anti-CD27 (M-T271), anti-CD8 (RPA-T8), anti-IgM (MHM88), anti-CD4 (RPA-T4). Samples were probed with 7-AAD to identify live cells. Data were acquired on a LSRII (BD Bioscience) and analyzed with FlowJo (TreeStar).

Human flow cytometry gating strategy. Live, singlet cells were identified as (1) Classical monocytes: CD14+CD16-; (2) Intermediate monocytes: CD14+CD16-; (3) Non-classical monocytes: CD14-CD16+, (4) Memory B cells: CD14-CD16-CD19+CD27+IgD-; (5) Non-class switched B cells: CD14-CD16-CD19+CD27+IgD+; (6) Naïve B cells: CD14-CD16-CD19+CD27-IgD+; (7) CD8+ T cells: CD14-CD16-CD19-CD3+CD4-CD8+; (8) CD4+ T cells: CD14-CD16-CD19-CD3+CD4+CD8-; (9) HSPCs: Lineage-CD34+. Lineage: CD2, CD3, CD4, CD7, CD8, CD10, CD11b, CD14, CD19, CD20, CD56, CD235. Viable cells were identified as unstained with 7AAD (Biolegend). Data were acquired on a LSRII (BD Biosciences) and analyzed with FlowJo (Tree Star).

Human Cell sorting. Cells suspensions were stained as above and HSPCs were sorted on a FACS Aria II cell sorter (BD Biosciences) directly into collection medium.

Enzymatic activity and histone acetylation. On sorted HSPCs HAT and HDAC activity along with H3 histone acetylation were measured using commercially available kits according to manufacturer's instructions. HAT kit (Sigma Aldrich, cat#EPI001), HDAC Kit (Sigma Aldrich, cat#CS1010), H3 acetylation kit (Abcam, cat#ab115102)

Human Energy Intake. In the human subjects study, which is ongoing, we collect data on food intake using 3-day 24-h food records. Participants are asked to record all foods they consume, in real time, on 3 non-

consecutive days (2 weekdays, 1 weekend). Participants are asked to provide detailed information on food brands, ingredients, and amounts and are provided with information on the use of common portion estimation tools. Food records are collected at week 0 (baseline), week 3, and week 6 (endpoint) of each phase. Nutrient analyses are completed in Nutrition Data System for Research (UMinn, Minneapolis, MN), and weekly averages are calculated from day-level data.

Human Adiposity. Total volume of adipose tissue and its distribution was measured at baseline and endpoint with MRI using procedures previously described(Shen *et al.*, 2004).

Data and materials availability: All data and methods are available and described within. Materials are available upon request.

Statistics

Results are shown as mean ± s.e.m. Statistical analysis was performed using GraphPad Prism 7 (Graphpad Software). Statistical tests included unpaired, two-tailed non-parametric Mann–Whitney U-tests (when Gaussian distribution was not assumed). For multiple comparisons of more than 2 groups, a non-parametric multiple-comparisons test comparing the mean rank of each group (when Gaussian distribution was not assumed) was used, along with one- or two-way ANOVAs followed by Tukey's test. For analysis of human data two-way ANOVAs were performed when comparing multiple groups and timepoints or two-tailed non-parametric Mann–Whitney U-tests when comparing two groups. Correlation was computed using linear regression. P values of 0.05 or less were considered to denote significance. Each mouse experiment was repeated independently at least two or more times with similar results.

AUTHOR CONTRIBUTIONS

Conceptualization: CSM, MGK, FMZ, DC, RIS, MN, KLJ, DTS, KN, MPSO, FKS
Data acquisition: CSM, MGK, FMZ, DC, GS, HA, PH, MZB, LPW, AGY, WCP, JEM, CTC, HJ, JD, SS
Data analysis: CSM, MGK, FMZ, DC, GS, HA, KN, MPSO, FKS
Methodology: CSM, MGK, FMZ, DC, GS, HA, RIS, MN, KLJ, DTS, KN, MPSO, FKS
Supervision: RIS, MN, KLJ, DTS, KN, MPSO, FKS
Writing: CSM, MGK, FZ, DC, KN, MPSO, FKS

ACKNOWLEDGEMENTS

We thank the HCI-CRM Flow Cytometry Core Facility at the Massachusetts General Hospital and the Flow Cytometry CoRE at the Icahn School of Medicine at Mount Sinai for assistance in cell sorting; the MGH NexGen sequencing and Bioinformatics facility for ATAC-seq experiments and analysis. This work was funded by the National Institutes of Health (NIH) K99/R00 HL151750, R01 HL158534, and the Cure Alzheimer's Fund (to C.S.M.); an Erwin Schrödinger Postdoctoral Fellowship J4645 (to M.G.K.); NIH T32 HL007343 and Russel Berrie Foundation Fellowship Award (to F.M.Z.); NIH P01 HL142494 and NIH R35 HL139598 (to M.N.); NIH Ruth L. Kirschstein National Research Service Award Individual Predoctoral Fellowship F31HL147364 (to J.E.M.); NIH R35 HL155670, R01 HL128226, and R01 HL142648 (to M.P.S.O); NIH National Center for Advancing Translational Sciences UL1TR001873; Cure Alzheimer's Fund, NIH R35 HL135752, P01 HL131478, P01 HL142494, and the Patricia and Scott Eston MGH Research Scholar (to F.K.S.). There are no competing financial interests.

DESCRIPTION OF SUPPLEMENTARY INFORMATION:

Supplementary tables and figures accompany this manuscript. They describe the influence of SF and RS on inflammation, LSK fitness, epigenetic rewiring, and adaptability; an analysis of mice treated with HDAC inhibitors; numerous quality control metrics of the clonal tracking system; the clonal frequency and diversity metrics of lymphocytes; and a description of the human trial and its participants along with an assessment of human leukocytosis with energy intake and adiposity.

REFERENCES

Besedovsky, L., Lange, T. and Haack, M. (2019) 'The Sleep-Immune Crosstalk in Health and Disease.', *Physiol Rev*, 99(3), pp. 1325–1380. doi: 10.1152/physrev.00010.2018.
Buisman, S. C. and de Haan, G. (2019) 'Epigenetic Changes as a Target in Aging Haematopoietic Stem Cells and Age-Related Malignancies.', *Cells*, 8(8). doi: 10.3390/cells8080868.

Buysse, D. J. *et al.* (1989) 'The Pittsburgh Sleep Quality Index: a new instrument for psychiatric practice and research.', *Psychiatry Research*, 28(2), pp. 193–213.
Carroll, J. E. *et al.* (2017) 'Epigenetic Aging and Immune Senescence in Women With Insomnia Symptoms: Findings From the Women's Health Initiative Study.', *Biol Psychiatry*, 81(2), pp. 136–144. doi: 10.1016/j.biopsych.2016.07.008.
Cedernaes, J. *et al.* (2018) 'Acute sleep loss results in tissue-specific alterations in genome-wide DNA methylation state and metabolic fuel utilization in humans', *Science Advances*. doi: 10.1126/sciadv.aar8590.
Chen, Y.-C. *et al.* (2019) 'Epigenetics: A Potential Mechanism Involved in the Pathogenesis of Various Adverse Consequences of Obstructive Sleep Apnea.', *International journal of molecular sciences*, 20(12). doi: 10.3390/ijms20122937.
Dashti, H. S. *et al.* (2021) 'Genetic determinants of daytime napping and effects on cardiometabolic health.', *Nature communications*, 12(1), p. 900. doi: 10.1038/s41467-020-20585-3.
Depner, C. M. *et al.* (2019) 'Ad libitum Weekend Recovery Sleep Fails to Prevent Metabolic Dysregulation during a Repeating Pattern of Insufficient Sleep and Weekend Recovery Sleep.', *Current biology : CB*, 29(6), pp. 957-967.e4. doi: 10.1016/j.cub.2019.01.069.
Dimitrov, S. *et al.* (2004) 'Sleep associated regulation of T helper 1/T helper 2 cytokine balance in humans.', *Brain, behavior, and immunity*, 18(4), pp. 341–348. doi: 10.1016/j.bbi.2003.08.004.
Dimitrov, S. *et al.* (2006) 'Sleep enhances IL-6 trans-signaling in humans.', *FASEB journal : official publication of the Federation of American Societies for Experimental Biology*, 20(12), pp. 2174–2176. doi: 10.1096/fj.06-5754fje.
Divangahi, M. *et al.* (2021) 'Trained immunity, tolerance, priming and differentiation: distinct immunological processes.', *Nature immunology*, 22(1), pp. 2–6. doi: 10.1038/s41590-020-00845-6.
Dorshkind, K. *et al.* (2020) 'Do haematopoietic stem cells age?', *Nature Reviews Immunology*, 20(3), pp. 196–202. doi: 10.1038/s41577-019-0236-2.
Durrett, R. (2012) *Essentials of Stochastic Processes*. 2nd edn. Springer-Verlag New York. doi: 10.1007/978-1-4614-3615-7.
Ewens, W. J. (2004) *Mathematical Population Genetics 1*. 2nd edn. Springer-Verlag New York. doi: 10.1007/978-0-387-21822-9.
Ferguson, T. *et al.* (2021) 'Annual, seasonal, cultural and vacation patterns in sleep, sedentary behaviour and physical activity: a systematic review and meta-analysis', *BMC Public Health*, 21(1), pp. 1–14. doi: 10.1186/s12889-021-11298-3.
Ford, E. S., Cunningham, T. J. and Croft, J. B. (2015) 'Trends in Self-Reported Sleep Duration among US Adults from 1985 to 2012.', *Sleep*, 38(5), pp. 829–832. doi: 10.5665/sleep.4684.
Friedman, E. M. *et al.* (2005) 'Social relationships, sleep quality, and interleukin-6 in aging women', *Proceedings of the National Academy of Sciences of the United States of America*, 102(51), pp. 18757–18762. doi: 10.1073/pnas.0509281102.
Full, K. M. *et al.* (2018) 'Validation of a physical activity accelerometer device worn on the hip and wrist against polysomnography', *Sleep Health*, 4(2), pp. 209–216. doi: 10.1016/j.sleh.2017.12.007.
Genovese, G. *et al.* (2014) 'Clonal Hematopoiesis and Blood-Cancer Risk Inferred from Blood DNA Sequence', *New England Journal of Medicine*. doi: 10.1056/nejmoa1409405.
Geovanini, G. R. *et al.* (2018) 'Elevations in neutrophils with obstructive sleep apnea: The Multi-Ethnic Study of Atherosclerosis (MESA)', *International Journal of Cardiology*. doi: 10.1016/j.ijcard.2017.10.121.
Heyde, A. *et al.* (2021) 'Increased stem cell proliferation in atherosclerosis accelerates clonal hematopoiesis', *Cell*, 184(5), pp. 1348-1361.e22. doi: 10.1016/j.cell.2021.01.049.
Hong, S. *et al.* (2005) 'The association between interleukin-6, sleep, and demographic characteristics.', *Brain, behavior, and immunity*, 19(2), pp. 165–172. doi: 10.1016/j.bbi.2004.07.008.
Horne, J. A. and Ostberg, O. (1976) 'A self assessment questionnaire to determine Morningness Eveningness in human circadian rhythms', *International Journal of Chronobiology*, 4(2), pp. 97–110.
Irwin, M. R. (2019) 'Sleep and inflammation: partners in sickness and in health', *Nature Reviews Immunology*. doi: 10.1038/s41577-019-0190-z.
Jaiswal, S. *et al.* (2014) 'Age-Related Clonal Hematopoiesis Associated with Adverse Outcomes', *New England Journal of Medicine*, 371(26), pp. 2488–2498. doi: 10.1056/nejmoa1408617.
Jaiswal, S. *et al.* (2017) 'Clonal Hematopoiesis and Risk of Atherosclerotic Cardiovascular Disease', *New England Journal of Medicine*. doi: 10.1056/nejmoa1701719.
Johns, M. W. (1991) 'A New Method for Measuring Daytime Sleepiness: The Epworth Sleepiness Scale', *Sleep*, 14(6), pp. 540–545. doi: 10.1093/sleep/14.6.540.

Kamel, N. S. and Gammack, J. K. (2006) ‘Insomnia in the elderly: cause, approach, and treatment.’, *Am J Med*, 119(6), pp. 463–469. doi: 10.1016/j.amjmed.2005.10.051.
Khan, N. *et al.* (2020) ‘M. tuberculosis Reprograms Hematopoietic Stem Cells to Limit Myelopoiesis and Impair Trained Immunity’, *Cell*, 183(3), pp. 752-770.e22. doi: 10.1016/j.cell.2020.09.062.
Lallukka, T. *et al.* (2012) ‘Sociodemographic and socioeconomic differences in sleep duration and insomnia-related symptoms in Finnish adults’, *BMC Public Health*, 12(1). doi: 10.1186/1471-2458-12-565.
Lange, T. *et al.* (2006) ‘Shift of monocyte function toward cellular immunity during sleep.’, *Archives of internal medicine*, 166(16), pp. 1695–1700. doi: 10.1001/archinte.166.16.1695.
Langer, G. and Filer, C. (2020) ‘2020 Sleep in America Poll – Sleepiness’, *Sleep Health*, 6(5), pp. e1–e3.
Leger, D. *et al.* (2020) ‘Napping and weekend catchup sleep do not fully compensate for high rates of sleep debt and short sleep at a population level (in a representative nationwide sample of 12,637 adults).’, *Sleep medicine*, 74, pp. 278–288. doi: 10.1016/j.sleep.2020.05.030.
Li, X. *et al.* (2019) ‘Association between sleep disordered breathing and epigenetic age acceleration: Evidence from the Multi-Ethnic Study of Atherosclerosis.’, *EBioMedicine*, 50, pp. 387–394. doi: 10.1016/j.ebiom.2019.11.020.
Libby, P. and Rocha, V. Z. (2018) ‘All roads lead to IL-6: A central hub of cardiometabolic signaling.’, *Int J Cardiol*, pp. 213–215. doi: 10.1016/j.ijcard.2018.02.062.
McAlpine, C. S. *et al.* (2019) ‘Sleep modulates haematopoiesis and protects against atherosclerosis’, *Nature*, 566(7744), pp. 383–387. doi: 10.1038/s41586-019-0948-2.
Mindur, J. E. and Swirski, F. K. (2019) ‘Growth factors as immunotherapeutic targets in cardiovascular disease’, *Arteriosclerosis, Thrombosis, and Vascular Biology*, 39(7), pp. 1275–1287. doi: 10.1161/ATVBAHA.119.311994.
Mitchell, E. *et al.* (2022) ‘Clonal dynamics of haematopoiesis across the human lifespan.’, *Nature*. doi: 10.1038/s41586-022-04786-y.
Morrison, S. J. *et al.* (1996) ‘The aging of hematopoietic stem cells’, *Nature Medicine*. doi: 10.1038/nm0996-1011.
Nachun, D. *et al.* (2021) ‘Clonal hematopoiesis associated with epigenetic aging and clinical outcomes.’, *Aging cell*, 20(6), p. e13366. doi: 10.1111/acel.13366.
Netzer, N. C. *et al.* (1999) ‘Using the Berlin Questionnaire To Identify Patients at Risk for the Sleep Apnea Syndrome’, *Annals of Internal Medicine*, 131(7), p. 485. doi: 10.7326/0003-4819-131-7-199910050-00002.
Nicodeme, E. *et al.* (2010) ‘Suppression of inflammation by a synthetic histone mimic’, *Nature*, 468(7327), pp. 1119–1123. doi: 10.1038/nature09589.
Ohayon, M. M. *et al.* (2004) ‘Meta-analysis of quantitative sleep parameters from childhood to old age in healthy individuals: Developing normative sleep values across the human lifespan’, *Sleep*, 27(7), pp. 1255–1273. doi: 10.1093/sleep/27.7.1255.
Pietras, E. M. *et al.* (2015) ‘Functionally Distinct Subsets of Lineage-Biased Multipotent Progenitors Control Blood Production in Normal and Regenerative Conditions’, *Cell Stem Cell*, 17(1), pp. 35–46. doi: 10.1016/j.stem.2015.05.003.
Poon, G. Y. P. *et al.* (2021) ‘Synonymous mutations reveal genome-wide levels of positive selection in healthy tissues.’, *Nature genetics*, 53(11), pp. 1597–1605. doi: 10.1038/s41588-021-00957-1.
Ridker, P. M. and Rane, M. (2021) ‘Interleukin-6 Signaling and Anti-Interleukin-6 Therapeutics in Cardiovascular Disease.’, *Circulation research*, 128(11), pp. 1728–1746. doi: 10.1161/CIRCRESAHA.121.319077.
Rodrigues, C. P., Shvedunova, M. and Akhtar, A. (2021) ‘Epigenetic Regulators as the Gatekeepers of Hematopoiesis’, *Trends in Genetics*, 37(2), pp. 125–142. doi: 10.1016/j.tig.2020.09.015.
Rossi, D. J. *et al.* (2005) ‘Cell intrinsic alterations underlie hematopoietic stem cell aging’, *Proceedings of the National Academy of Sciences of the United States of America*. doi: 10.1073/pnas.0503280102.
Ruiz, F. S. *et al.* (2012) ‘Immune alterations after selective rapid eye movement or total sleep deprivation in healthy male volunteers.’, *Innate immunity*, 18(1), pp. 44–54. doi: 10.1177/1753425910385962.
Samanta, A. *et al.* (2008) ‘TGF-beta and IL-6 signals modulate chromatin binding and promoter occupancy by acetylated FOXP3.’, *Proceedings of the National Academy of Sciences of the United States of America*, 105(37), pp. 14023–14027. doi: 10.1073/pnas.0806726105.
Shen, W. *et al.* (2004) ‘Visceral adipose tissue: relations between single-slice areas and total volume.’, *The American journal of clinical nutrition*, 80(2), pp. 271–278. doi: 10.1093/ajcn/80.2.271.
Shen, Y. J. *et al.* (2021) ‘Progression signature underlies clonal evolution and dissemination of multiple myeloma’, *Blood*, 137(17), pp. 2360–2372. doi: 10.1182/blood.2020005885.

Snippert, H. J. *et al.* (2010) 'Intestinal crypt homeostasis results from neutral competition between symmetrically dividing Lgr5 stem cells.', *Cell*, 143(1), pp. 134–144. doi: 10.1016/j.cell.2010.09.016.
Unruh, M. L. *et al.* (2008) 'Subjective and objective sleep quality and aging in the sleep heart health study', *Journal of the American Geriatrics Society*, 56(7), pp. 1218–1227. doi: 10.1111/j.1532-5415.2008.01755.x.
Vallat, R. *et al.* (2020) 'Broken sleep predicts hardened blood vessels', *PLoS Biology*, 18(6), pp. 1–11. doi: 10.1371/journal.pbio.3000726.
Watson, N. F. *et al.* (2015) 'Joint Consensus Statement of the American Academy of Sleep Medicine and Sleep Research Society on the Recommended Amount of Sleep for a Healthy Adult: Methodology and Discussion', *Journal of Clinical Sleep Medicine*. doi: 10.5664/jcsm.4950.
Weber, G. F. *et al.* (2015) 'Interleukin-3 amplifies acute inflammation and is a potential therapeutic target in sepsis', *Science*, 347(6227), pp. 1260–1265. doi: 10.1126/science.aaa4268.
Yu, V. W. C. *et al.* (2016) 'Epigenetic Memory Underlies Cell-Autonomous Heterogeneous Behavior of Hematopoietic Stem Cells', *Cell*, 167(5), pp. 1310-1322.e17. doi: 10.1016/j.cell.2016.10.045.
Zink, F. *et al.* (2017) 'Clonal hematopoiesis, with and without candidate driver mutations, is common in the elderly', *Blood*, 130(6), pp. 742–752. doi: 10.1182/blood-2017-02-769869.

FIGURE LEGENDS

Figure 1. Sleep exerts a prolonged influence on hematopoiesis. (A) Quantification of wake bouts (transitions from sleep to wake states), during the resting (light) period along with a representative hypnogram in control (C) and sleep fragmented (SF) mice. (n=4 mice per group). (**B)** Quantification of minutes per hour in slow wave sleep (SWS), rapid eye movement (REM) sleep, and awake time, along with representative EEG and EMG traces, in control and SF animals over 24 hours. (n=4 mice per group). **(C)** Quantification of resting period wake bouts over 16 weeks of SF followed by 10 weeks of recovery sleep (RS). (n=4 mice per group). **(D)** Enumeration of blood Ly6C^{hi} monocytes and BM LSKs, along with LSK BrdU incorporation in control mice, SF mice, and mice exposed to 16 weeks of SF followed by 4 weeks of RS. (n=5-6 mice per group). **(E)** Enumeration of blood Ly6C^{hi} monocytes and BM LSKs, along with LSK proliferation in a distinct cohort of control mice and mice exposed to 16 weeks of SF followed by 10 weeks of RS. (n=4 mice per group). **(F)** BrdU incorporation into LSKs from control (CD45.1) or SF (CD45.2) mice three weeks after competitive 1:1 LSK transplantation into a UbiGFP mouse sleeping habitually. (n=6-7 mice per group). **(G)** Competitive 1:1 transplantation of LSKs from control (CD45.1) or SF (CD45.2) mice into UbiGFP recipient mice and quantification of CD45.1/2 chimerism among blood leukocytes and Ly6C^{hi} monocytes up to 24 weeks after transplantation. (n=8 mice per group). Mean±s.e.m. *p<0.05, **p<0.01

Figure 2. Sleep programs the LSK epigenome and confers adaptability. (A) Experimental schematic. **(B)** Distribution of differentially accessible (DA, Log2FC>2, p<0.05, red circles) enhancer loci in control and SF LSKs. **(C)** Accessibility heat map of DA enhancer loci between control and SF LSKs and corresponding accessibility in RS group, indicating preserved signature of loci not significantly different (Log2FC<2, p<0.05) between SF and RS. **(D)** KEGG pathway analysis of the retained signature. **(E)** Heatmap of enhancer loci associated with genes important to lymphocyte differentiation, myeloid differentiation, and cyclin signaling. For ATACseq analysis, n=2 mice per group, repeated twice, for a total of n=4 per group. Representative peak map **(F)** and qPCR analysis of *Cdkn1b*, *Cdkn2b*, *Cdkal1, Klf9*, and *Klf3* expression in LSKs of control, SF, and SF+RS mice (n=4-7 mice per group). **(H)** Experimental set up, cecal ligation and puncture=CLP. **(I)** Blood bacteremia and Ly6C^{hi} monocytes along with BM LSKs and proliferation 24 hours after CLP. (n=4-8 mice per group). **J.** Plasma cytokine levels. (n=8 mice per group). **(K)** Clinical score (n=8 mice per group) and survival (n=10 mice per group) post-CLP. **(L)** Schematic of experimental design. **(M)** Blood monocyte numbers immediately prior to and **(N)** 24 hours after the CLP. (n=3-5 mice per group). **(O)** BM LSKs and proliferation 24 hours after CLP. (n=5 mice per group). **(P)** Plasma cytokine levels and clinical score after CLP. n=5 mice per group). Mean±s.e.m. *p<0.05, **p<0.01, ***p<0.001, ****p<0.0001

Figure 3. Sleep-controlled immune adaptability is blunted by epigenetic modifiers. (A) Experimental schematic of 4-phenylbutyrate (4PBA) delivery. **(B)** Blood monocyte numbers and BM LSKs and proliferation 24 hours after CLP. (n=4-5 mice per group). **(C)** Plasma cytokine levels 24 hours after CLP. (n=4-5 mice per group). **(D)** Experimental schematic of iBet delivery. **(E)** Blood monocytosis 24 hrs after CLP. (n=4-5 mice per

group). **(F)** BM LSKs and proliferation 24 hrs after CLP. (n=4-5 mice per group). **(G)** Plasma cytokine levels 24 hrs after CLP. (n=4-5 mice per group). Mean±s.e.m. *p<0.05

Figure 4. Sleep maintains hematopoietic diversity and limits neutral drift. (A) Experimental set up to generate tagged LSKs and transplantation into recipient mice. **(B)** representative flow cytometry plots of leukocyte clusters in the blood. **(C)** Change in cluster frequency relative to baseline, mean cluster frequency, and variance of cluster frequencies of monocytes with 4 or more tags. **(D)** Change in cluster frequency relative to baseline, mean cluster frequency, and variance of cluster frequencies of neutrophils with 4 or more tags. **(E)** Simpson's diversity Index among all 127 tagged monocyte clusters. **(F)** Simpson's diversity Index among all 127 tagged neutrophil clusters. **(G)** Variance of LSK frequencies (p=0.16) and Simpson's diversity index (p=0.27) among 127 tagged LSK clusters after 18 weeks of SF. **(H)** Simpson diversity Index of BM LSKs and blood monocytes at sacrifice. **(I)** Enumeration of BM LSKs in recipient mice. **(J)** LSK proliferation after 18 weeks of SF. In all panels, n=5 mice per group, except J where n=6 mice per group. Mean±s.e.m. *p<0.05, **p<0.01, ***p<0.001

Figure 5. Human sleep restriction promotes monocytosis and shapes the HSPC epigenome. (A) Schematic of cross-over sleep restriction study (n=14, HS=habitual sleep, SR=sleep restriction). **(B)** Total sleep time of subjects during the habitual sleep phase and the sleep restriction phase measured weekly and averaged over the phase. **(C)** Enumeration of leukocyte populations in the blood during the morning (M) and evening (E) at the completion of each phase. **(D)** Enumeration of Lineage$^-$CD34$^+$ hematopoietic stem and progenitor cells (HSPCs). **(E)** HAT and HDAC activity in Lineage$^-$CD34$^+$ HPCs at the evening time point. **(F)** Histone H3 acetylation in Lineage$^-$CD34$^+$ HSPCs at the evening time point. **(G)** Mean fluorescence intensity (MFI) of CD115 and CD123 on HSPCs at the evening time point. Mean±s.e.m. *p<0.05, ***p<0.001

SUPPLEMENTAL MATERIAL LEGENDS

Table S1. LSK cluster frequency. Frequencies of fluorescently tagged clusters among transplanted LSKs.

Table S2. Number of LSKs in recipient control and SF mice. Total number of BM LSKs was calculated based on the BM of one leg representing 8% of the total BM. Fluorescent tagging recipient mice.

Table S3. Human subject characteristics at baseline. [a]Derived from 2 wk wrist actigraphy (Actigraph GT3X+; ActiLife software) and nightly sleep diaries. [b]Global score from the Pittsburgh Sleep Quality Index; possible score range is 0-21 with lower scores representing better sleep quality.

Figure S1. Influence of SF and RS on inflammation, LSK fitness, epigenetic rewiring, and adaptability. (A) Experimental design. **(B)** Growth factor levels in the BM fluid. **(C)** Cytokine, growth factor, and corticosterone levels in plasma of control and SF mice (n=3-14 mice per group). **(D)** Body weight measurement of control and SF mice. **(E)** Experimental schematic of control mice and mice exposed to 16 weeks of SF followed by 10 weeks of RS. **(F)** Growth factor levels in the BM fluid. **(G)** Levels of plasma cytokines, growth factors, and corticosterone (n=4 mice per group). **(H)** Body weight of control and SF+RS mice (n=4 mice per group). **(I)** Engraftment of control GFP$^-$CD45.1 and SF GFP$^-$CD45.2 LSKs in the BM 24 hours after transplantation. **(J)** Competitive 1:1 transplantation of LSKs from control (GFP$^+$CD45.2) or SF (GFP$^-$CD45.2) mice into a CD45.1 recipient mice and quantification of GFP$^+$ vs. GFP$^-$ chimerism among blood Ly6C^{hi} monocytes 18 weeks after transplantation. (n=7 mice per group). **(K)** Histone acetyltransferase (HAT) and histone deacetylase (HDAC) activity in BM lineage$^-$cKit$^+$ cells. n=4-5 mice per group. **(L)** Genomic distribution of accessibility peaks in LSK ATACseq data. **(M)** Analysis of hematopoietic growth factors and corticosterone levels in plasma of control and SF+RS mice after CLP (n=4-8 mice per group). **(N)** Schematic of repeated SF episodes. Blood monocytosis during first or second SF exposure. (n=5 mice per group) and BM LSKs and proliferation 5 weeks after initiating first or second SF exposure (n=4 mice per group). ns=not significant, Mean±s.e.m. *p<0.05 ***p<0.001

Figure S2. Analysis of mice treated with 4PBA. (A) Experimental design of 4PBA treatment during weeks 8 through 16 of control sleep or SF. **(B)** Body weight, data of C and SF mice are as in Fig S1 (n=5-6 mice per group). **(C)** Proportion of BM LSKs (n=3-5 mice per group). **(D)** Expression of *Cdkn1b, Cdkn2b, Cdkal1, Klf3,*

and *Klf9* genes in sorted LSKs, data from control and SF mice are as in Fig 2G (n=4-7 mice per group). ns=not significant.

Figure S3. Cluster size and distribution and correlation of cluster frequencies in the BM and blood. Distribution of tagged cluster frequency among **(A)** LSKs and **(B)** blood leukocytes at baseline. **(C)** Number of clusters detected at baseline among blood monocytes, neutrophils, T cells and B cells. Correlation of cluster frequency between BM LSKs and blood monocytes, and BM LSKs and blood neutrophils in each mouse at **(D)** baseline (correlating transplanted LSKs with blood cells 6 weeks after transplantation, prior to starting SF) and **(E)** after 18 weeks of SF or habitual sleep. n=5 mice per group. M=mouse.

Figure S4. Influence of sleep on lymphocyte diversity. (A) Change in cluster frequency, mean cluster frequency, and variance of detectable B cell clusters with 4 or more tags. **(B)** Simpson's diversity Index of B cells. **(C)** Change in cluster frequency, mean cluster frequency, and variance of of detectable T cell clusters with 4 or more tags. **(D)** Simpson's diversity Index of T cells. n=5 mice per group. **(E)** Change in Simpson's diversity index (SDI) from BM LSKs to blood neutrophils, B cells, and T cells. n=5 mice per group. ns=not significant. Mean±s.e.m

Figure S5. Human study. (A) Flow chart of the human study. Correlation of evening blood monocytes **(B)** and HSPCs **(C)** with energy intake and total adiposity at the completion of the HS and SR phases in human subject in which these parameters were available.

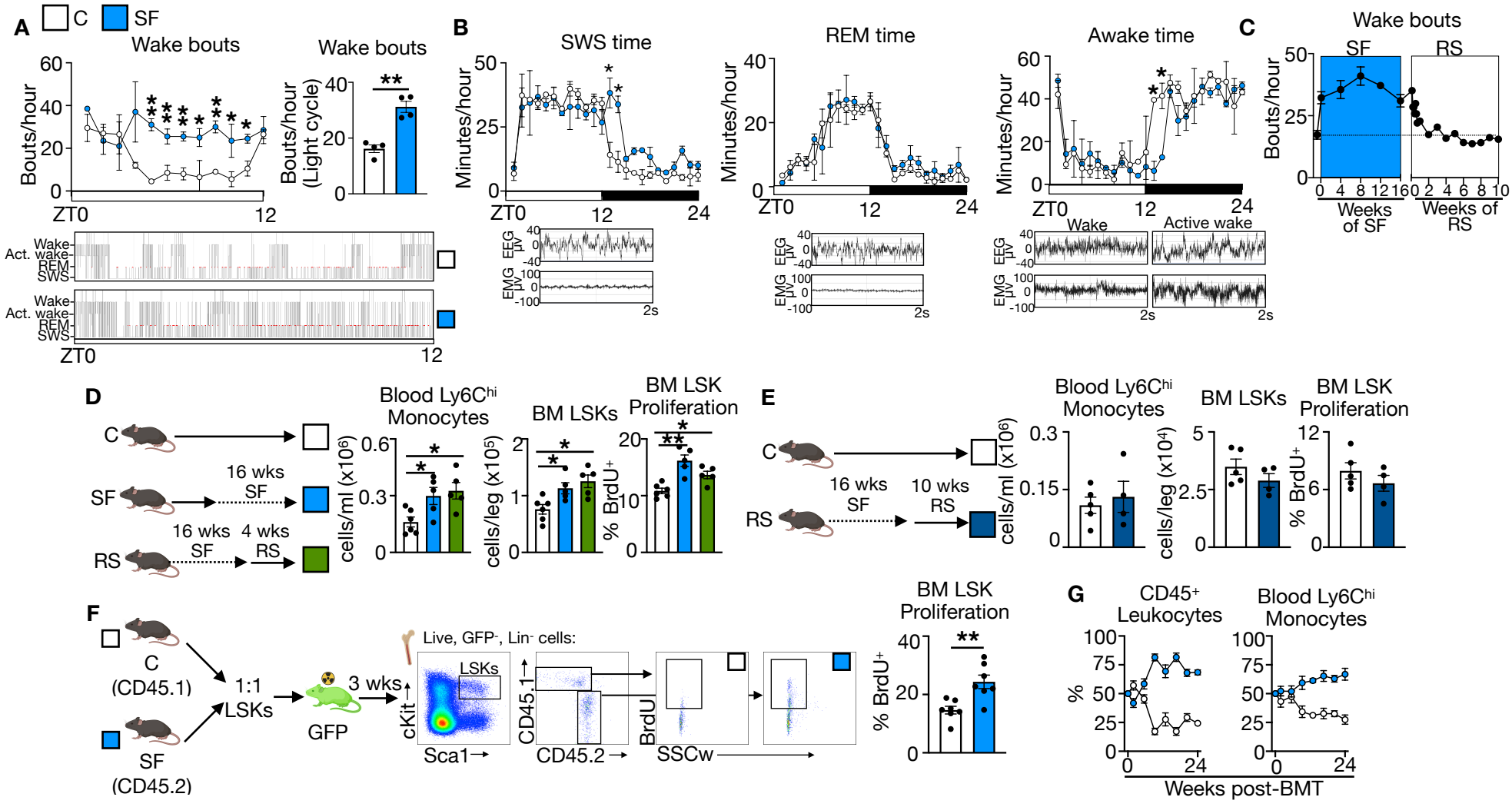
A
C
SF
Wake bouts
Bouts/hour
ZT0
12
Wake bouts
Bouts/hour (Light cycle)
Wake
Act. wake
REM
SWS
B
SWS time
REM time
Awake time
Minutes/hour
EEG
EMG
Active wake
2s
C
Wake bouts
SF
RS
Weeks of SF
Weeks of RS
D
Blood Ly6C^hi Monocytes
BM LSKs
BM LSK Proliferation
cells/ml (x10^6)
cells/leg (x10^5)
% BrdU+
16 wks SF
16 wks SF
4 wks RS
E
Blood Ly6C^hi Monocytes
BM LSKs
BM LSK Proliferation
16 wks SF
10 wks RS
F
C (CD45.1)
SF (CD45.2)
1:1 LSKs
3 wks
GFP
Live, GFP-, Lin- cells:
LSKs
cKit
Sca1
CD45.1
CD45.2
BrdU
SSCw
BM LSK Proliferation
G
CD45+ Leukocytes
Blood Ly6C^hi Monocytes
%
Weeks post-BMT

Figure 1

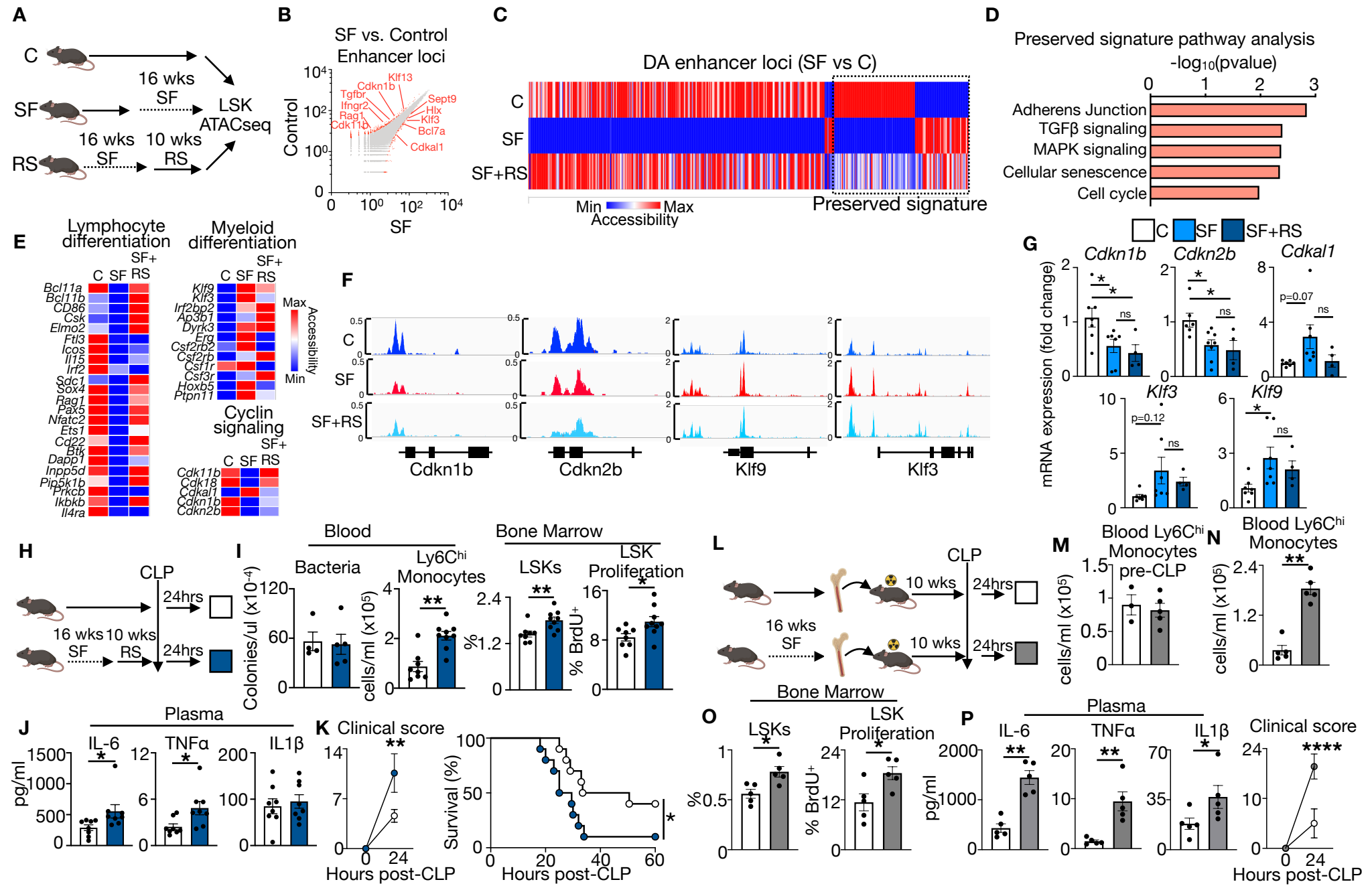
A
C
SF
RS
16 wks SF
LSK ATACseq
16 wks SF
10 wks RS
B
SF vs. Control Enhancer loci
Control
SF
Klf13
Cdkn1b
Tgfbr
Ifngr2
Rag1
Cdk11b
Sept9
Hlx
Klf3
Bcl7a
Cdkal1
C
DA enhancer loci (SF vs C)
SF+RS
Min
Max
Accessibility
Preserved signature
D
Preserved signature pathway analysis
-log10(pvalue)
Adherens Junction
TGFβ signaling
MAPK signaling
Cellular senescence
Cell cycle
E
Lymphocyte differentiation
Myeloid differentiation
Cyclin signaling
SF+
Bcl11a
Bcl11b
CD86
Csk
Elmo2
Ftl3
Icos
Il15
Irf2
Sdc1
Sox4
Rag1
Pax5
Nfatc2
Ets1
Cd22
Btk
Dapp1
Inpp5d
Pip5k1b
Prkcb
Ikbkb
Il4ra
Klf9
Klf3
Irf2bp2
Ap3b1
Dyrk3
Erg
Csf2rb2
Csf2rb
Csf1r
Csf3r
Hoxb5
Ptpn11
Cdk11b
Cdk18
Cdkal1
Cdkn1b
Cdkn2b
Max
Min
Accessibility
F
C
SF
SF+RS
Cdkn1b
Cdkn2b
Klf9
Klf3
G
C
SF
SF+RS
mRNA expression (fold change)
Cdkn1b
Cdkn2b
Cdkal1
Klf3
Klf9
p=0.07
p=0.12
ns
H
CLP
24hrs
16 wks SF
10 wks RS
I
Blood
Bone Marrow
Bacteria
Colonies/ul (x10-4)
Ly6Chi Monocytes
cells/ml (x10^5)
LSKs
%
LSK Proliferation
% BrdU+
L
CLP
10 wks
24hrs
16 wks SF
M
Blood Ly6Chi Monocytes pre-CLP
cells/ml (x10^5)
N
Blood Ly6Chi Monocytes
cells/ml (x10^5)
J
Plasma
IL-6
TNFα
IL1β
pg/ml
K
Clinical score
Hours post-CLP
Survival (%)
O
Bone Marrow
LSKs
%
LSK Proliferation
% BrdU+
P
Plasma
IL-6
TNFα
IL1β
pg/ml
Clinical score
Hours post-CLP

Figure 2

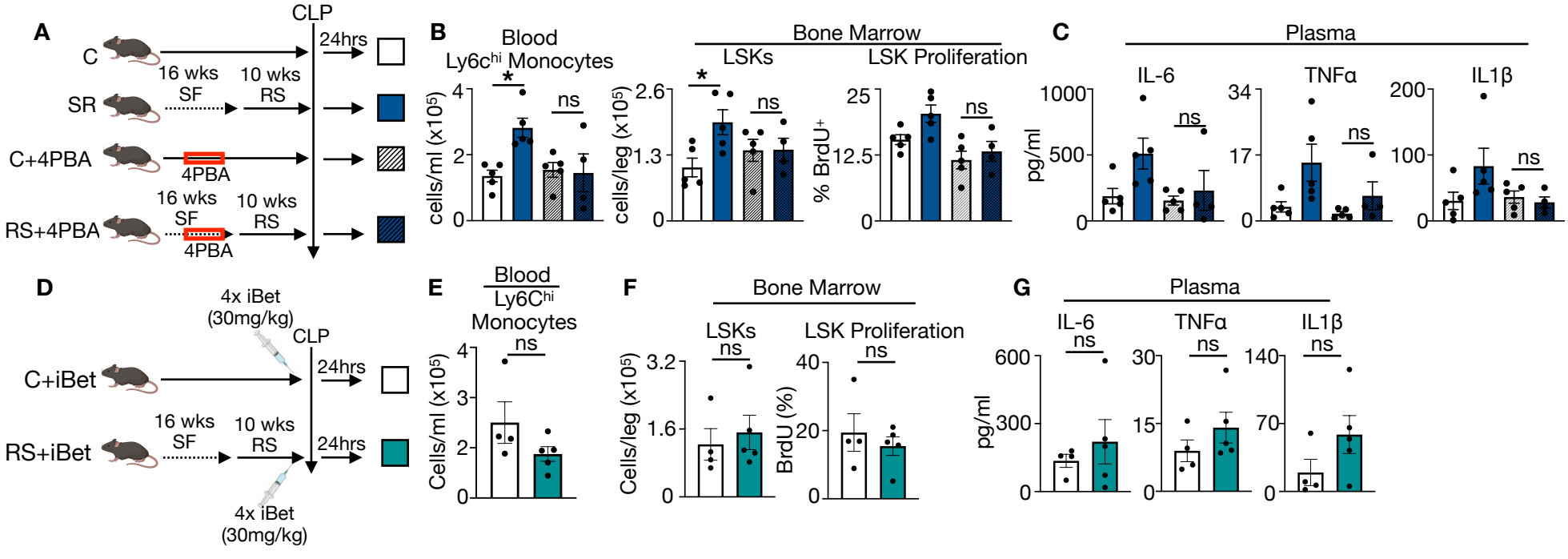
A
CLP
C
SR
C+4PBA
RS+4PBA
16 wks SF
10 wks RS
24hrs
4PBA
B
Blood
Ly6c^hi Monocytes
cells/ml (x10^5)
Bone Marrow
LSKs
LSK Proliferation
cells/leg (x10^5)
% BrdU+
ns
C
Plasma
IL-6
TNFα
IL1β
pg/ml
D
4x iBet (30mg/kg)
C+iBet
RS+iBet
E
Blood
Ly6C^hi Monocytes
Cells/ml (x10^5)
F
Bone Marrow
LSKs
LSK Proliferation
Cells/leg (x10^5)
BrdU (%)
G
Plasma
IL-6
TNFα
IL1β
pg/ml

Figure 3

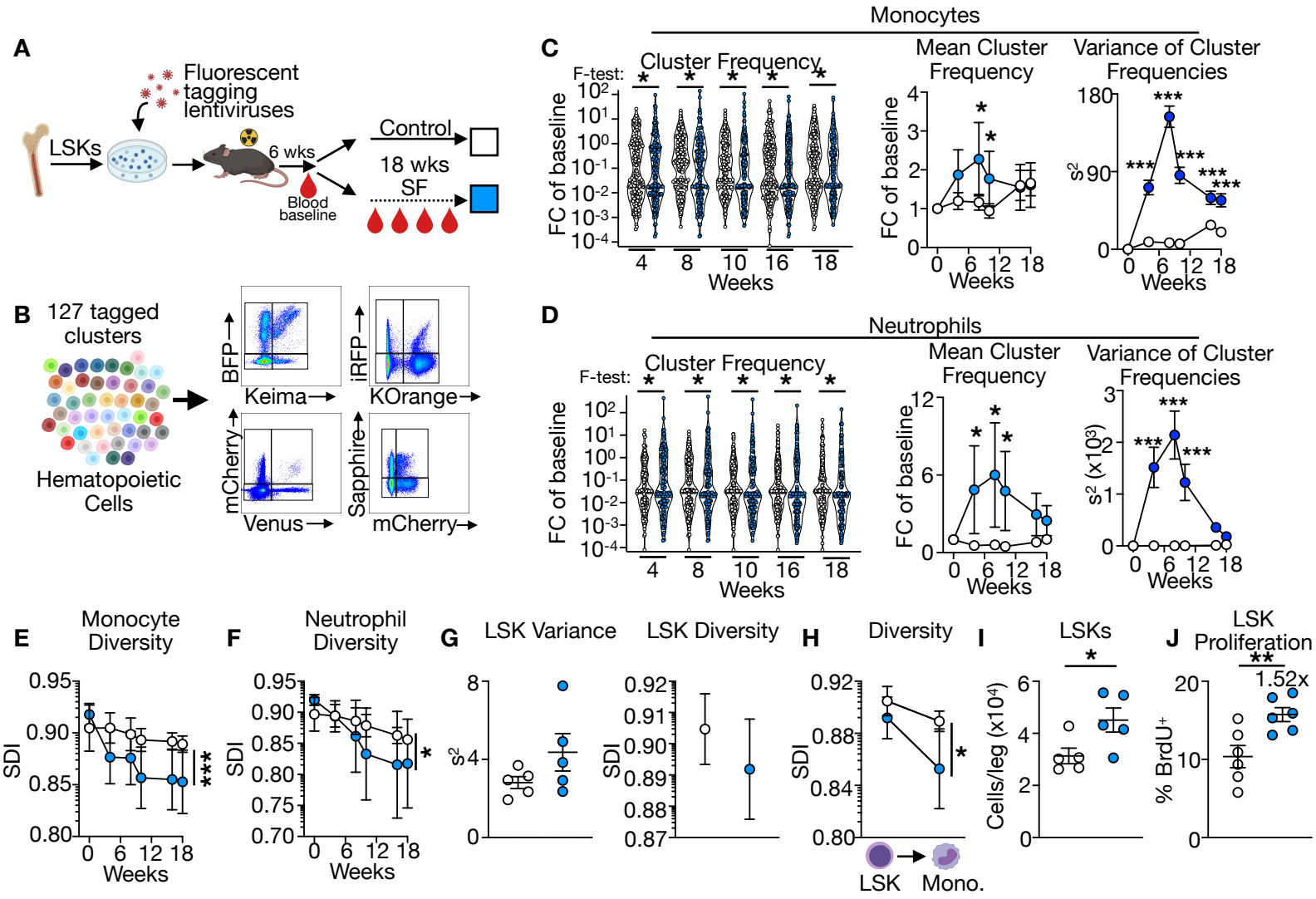
A
Fluorescent tagging lentiviruses
LSKs
6 wks
Control
18 wks SF
Blood baseline
B
127 tagged clusters
Hematopoietic Cells
BFP
Keima
iRFP
KOrange
mCherry
Venus
Sapphire
mCherry
C
Monocytes
Cluster Frequency
F-test:
FC of baseline
Weeks
Mean Cluster Frequency
Variance of Cluster Frequencies
D
Neutrophils
Cluster Frequency
Mean Cluster Frequency
Variance of Cluster Frequencies
E
Monocyte Diversity
SDI
Weeks
F
Neutrophil Diversity
G
LSK Variance
LSK Diversity
H
Diversity
LSK
Mono.
I
LSKs
Cells/leg (x10⁴)
J
LSK Proliferation
1.52x
% BrdU⁺

Figure 4

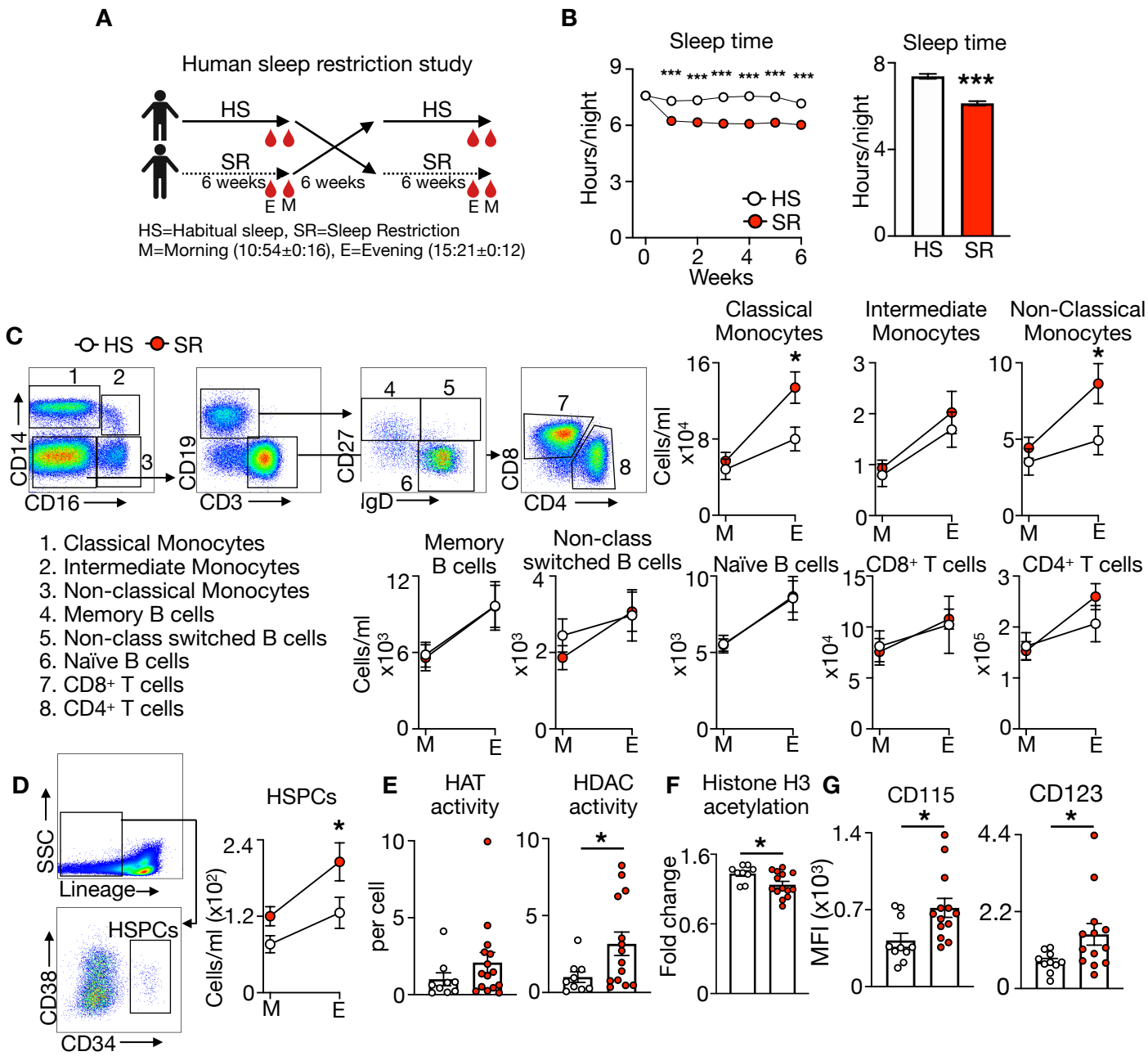
A
Human sleep restriction study
HS
SR
6 weeks
6 weeks
6 weeks
E M
E M
HS=Habitual sleep, SR=Sleep Restriction
M=Morning (10:54±0:16), E=Evening (15:21±0:12)
B
Sleep time
Hours/night
Weeks
HS
SR
Sleep time
Hours/night
C
HS SR
CD14
CD16
CD19
CD3
CD27
IgD
CD8
CD4
1. Classical Monocytes
2. Intermediate Monocytes
3. Non-classical Monocytes
4. Memory B cells
5. Non-class switched B cells
6. Naïve B cells
7. CD8⁺ T cells
8. CD4⁺ T cells
Classical Monocytes
Intermediate Monocytes
Non-Classical Monocytes
Cells/ml
Memory B cells
Non-class switched B cells
Naïve B cells
CD8⁺ T cells
CD4⁺ T cells
D
SSC
Lineage
HSPCs
CD38
CD34
HSPCs
Cells/ml (x10²)
E
HAT activity
HDAC activity
per cell
F
Histone H3 acetylation
Fold change
G
CD115
CD123
MFI (x10³)

Figure 5

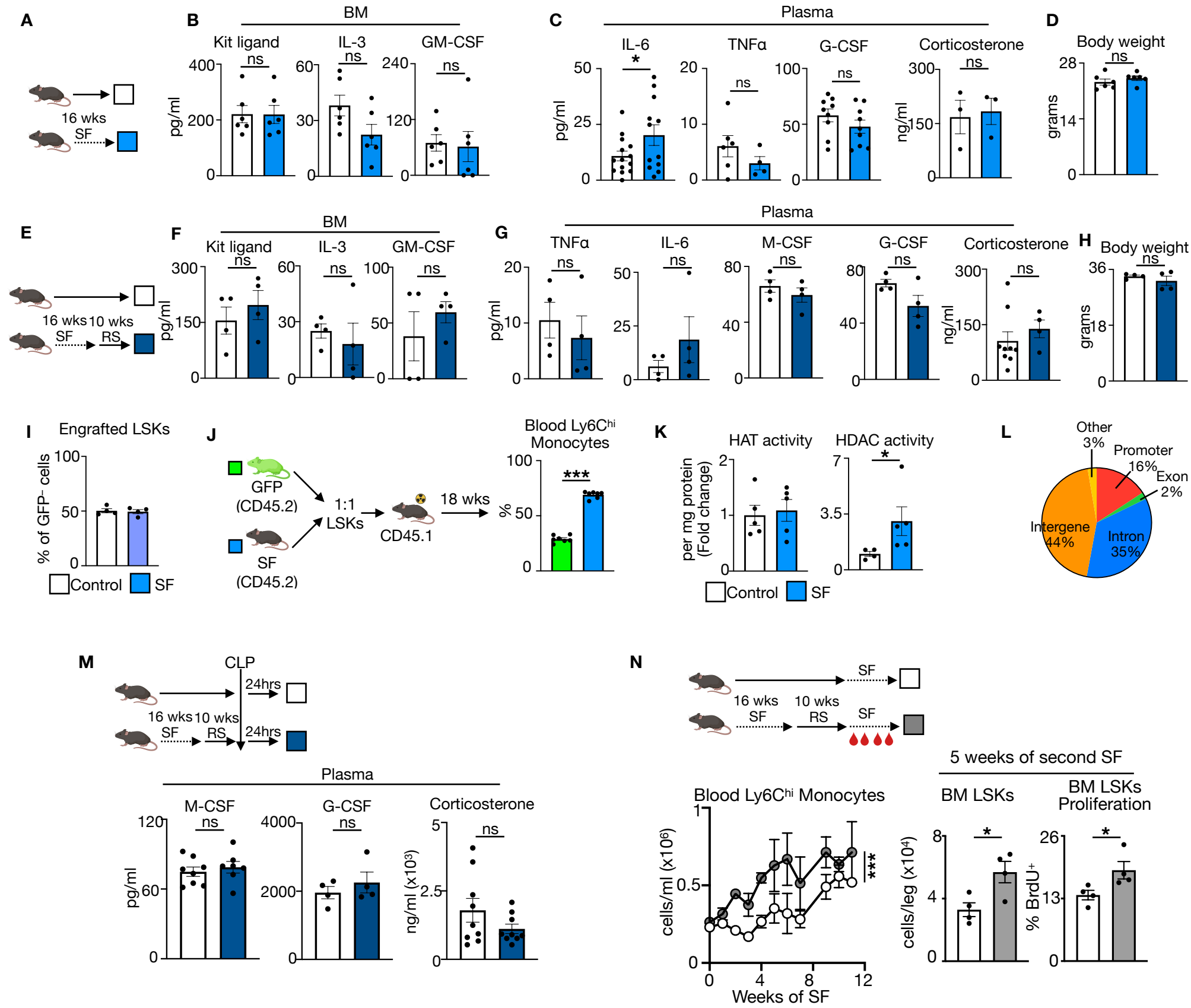
A
16 wks
SF
B
BM
Kit ligand
IL-3
GM-CSF
pg/ml
ns
C
Plasma
IL-6
TNFα
G-CSF
Corticosterone
pg/ml
ng/ml
D
Body weight
grams
E
16 wks
SF
10 wks
RS
F
BM
Kit ligand
IL-3
GM-CSF
G
Plasma
TNFα
IL-6
M-CSF
G-CSF
Corticosterone
H
Body weight
I
Engrafted LSKs
% of GFP- cells
Control
SF
J
GFP
(CD45.2)
SF
(CD45.2)
1:1
LSKs
CD45.1
18 wks
Blood Ly6C^hi
Monocytes
%
***
K
HAT activity
HDAC activity
per mg protein
(Fold change)
Control
SF
L
Other
3%
Promoter
16%
Exon
2%
Intergene
44%
Intron
35%
M
CLP
24hrs
16 wks
SF
10 wks
RS
24hrs
N
SF
16 wks
SF
10 wks
RS
SF
5 weeks of second SF
Plasma
M-CSF
G-CSF
Corticosterone
pg/ml
ng/ml (x10³)
Blood Ly6C^hi Monocytes
cells/ml (x10⁶)
Weeks of SF
BM LSKs
BM LSKs
Proliferation
cells/leg (x10⁴)
% BrdU⁺

Figure S1

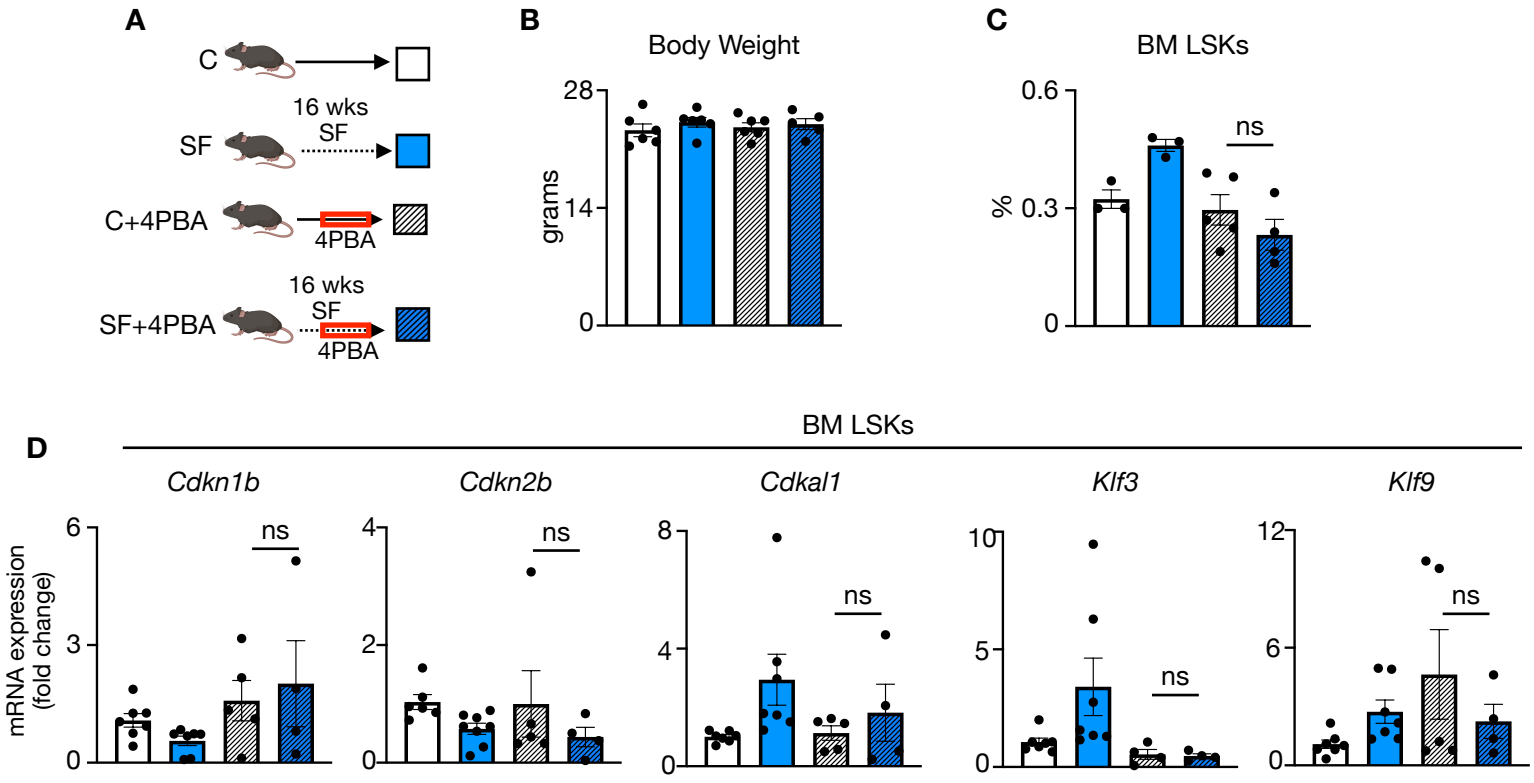
A
C
16 wks
SF
SF
C+4PBA
4PBA
16 wks
SF
SF+4PBA
4PBA
B
Body Weight
grams
28
14
0
C
BM LSKs
%
0.6
0.3
0
ns
D
BM LSKs
Cdkn1b
Cdkn2b
Cdkal1
Klf3
Klf9
mRNA expression
(fold change)
6
3
0
4
2
0
8
4
0
10
5
0
12
6
0
ns

Figure S2

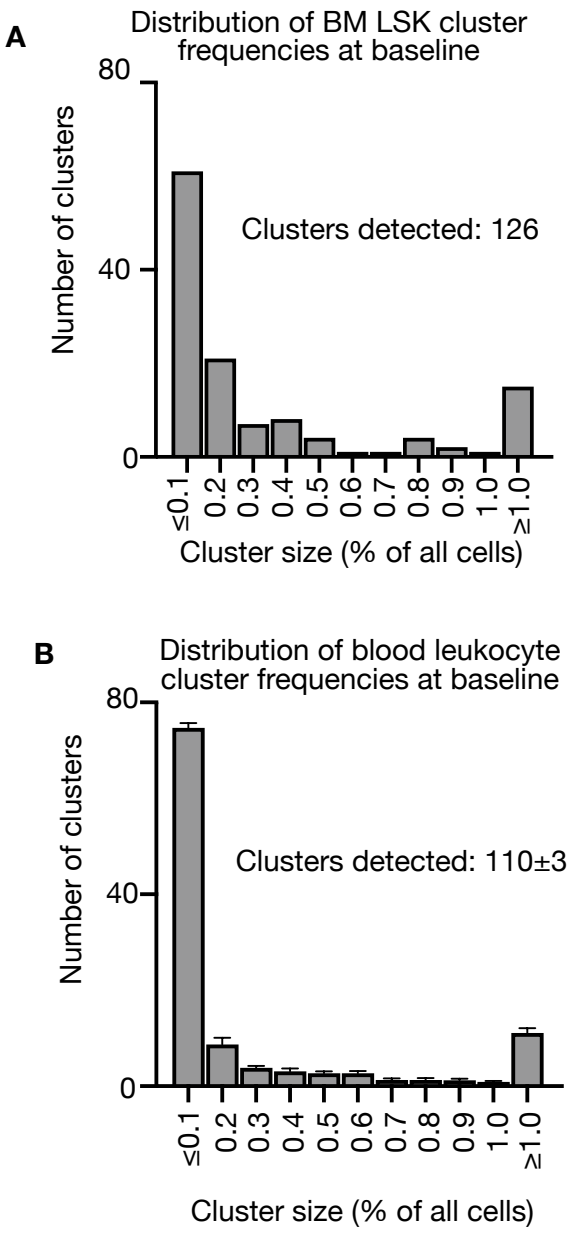
A
Distribution of BM LSK cluster frequencies at baseline
Number of clusters
Clusters detected: 126
Cluster size (% of all cells)
B
Distribution of blood leukocyte cluster frequencies at baseline
Number of clusters
Clusters detected: 110±3
Cluster size (% of all cells)

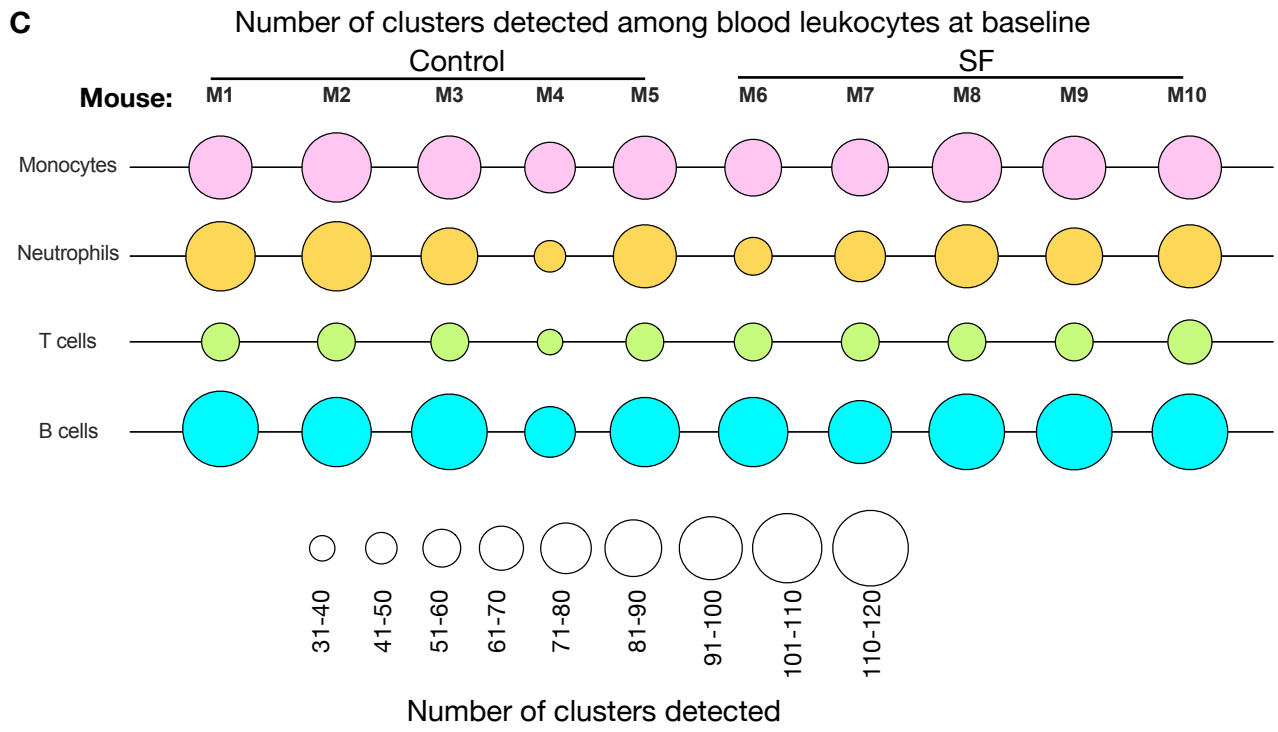
C
Number of clusters detected among blood leukocytes at baseline
Control
SF
Mouse:
M1
M2
M3
M4
M5
M6
M7
M8
M9
M10
Monocytes
Neutrophils
T cells
B cells
31-40
41-50
51-60
61-70
71-80
81-90
91-100
101-110
110-120
Number of clusters detected

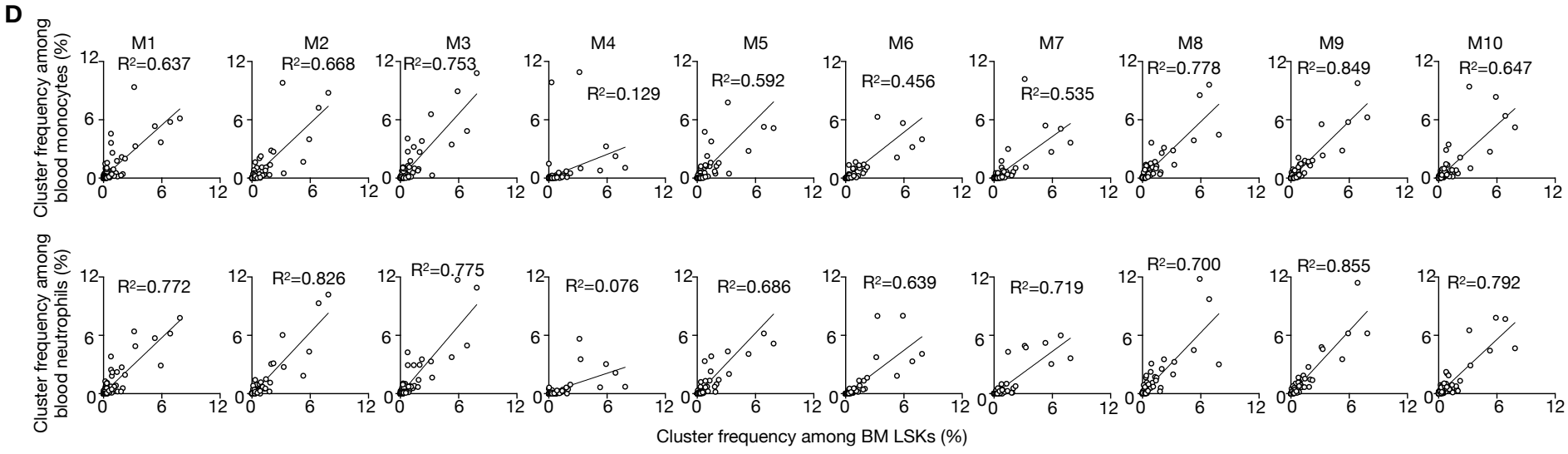
D
Cluster frequency among blood monocytes (%)
Cluster frequency among blood neutrophils (%)
Cluster frequency among BM LSKs (%)

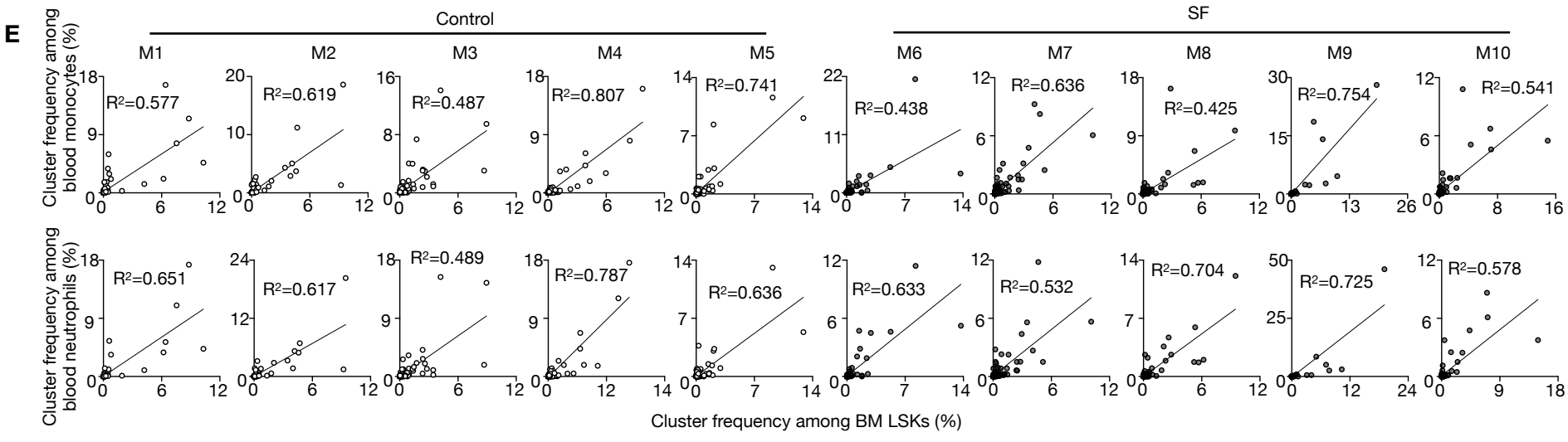
E
Control
SF
Cluster frequency among blood monocytes (%)
Cluster frequency among blood neutrophils (%)
Cluster frequency among BM LSKs (%)

Figure S3

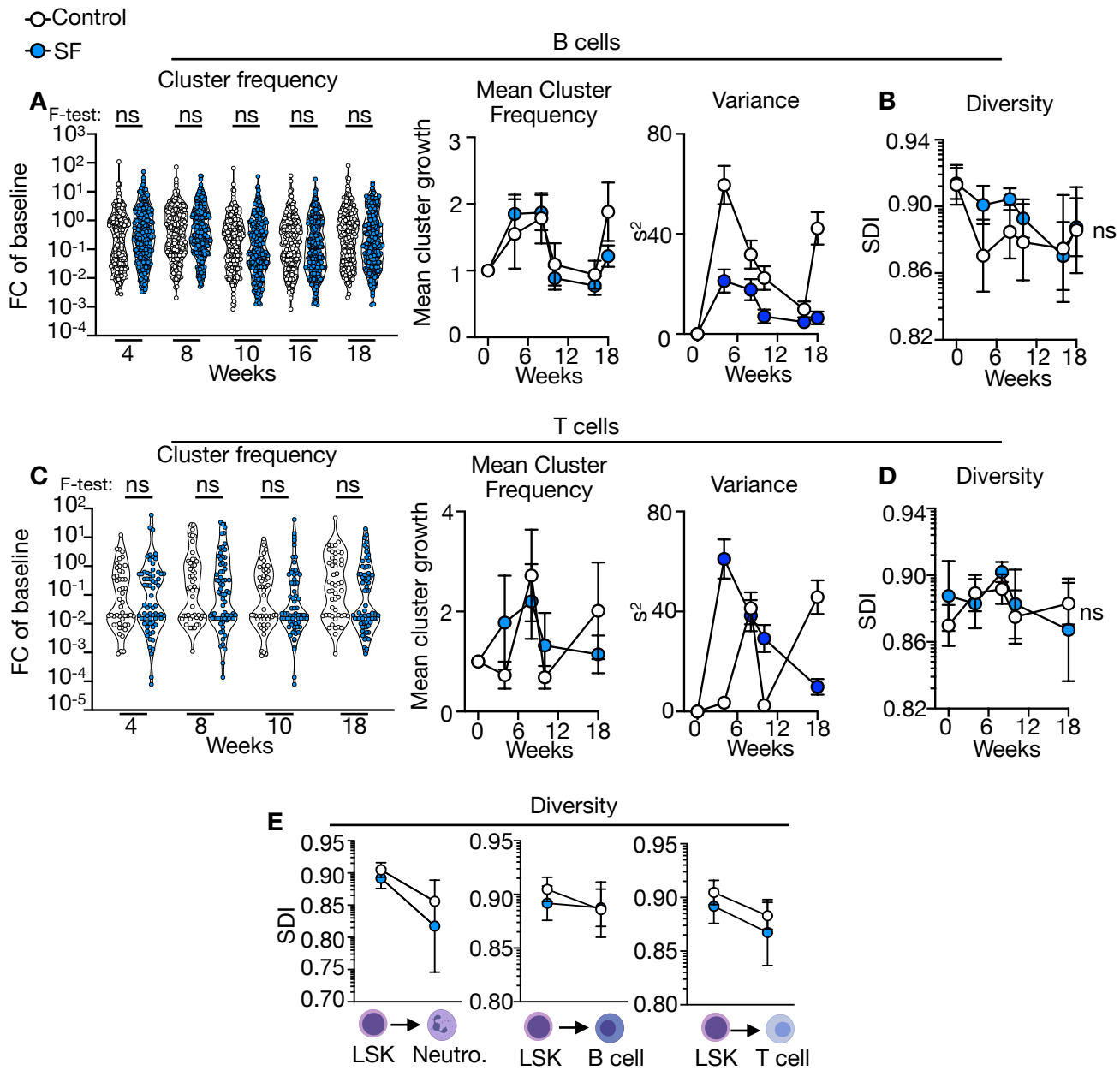
Control
SF
B cells
Cluster frequency
A
F-test: ns ns ns ns ns
FC of baseline
Weeks
Mean Cluster Frequency
Mean cluster growth
Variance
s²
B
Diversity
SDI
ns
T cells
C
D
E
LSK Neutro.
LSK B cell
LSK T cell

Figure S4

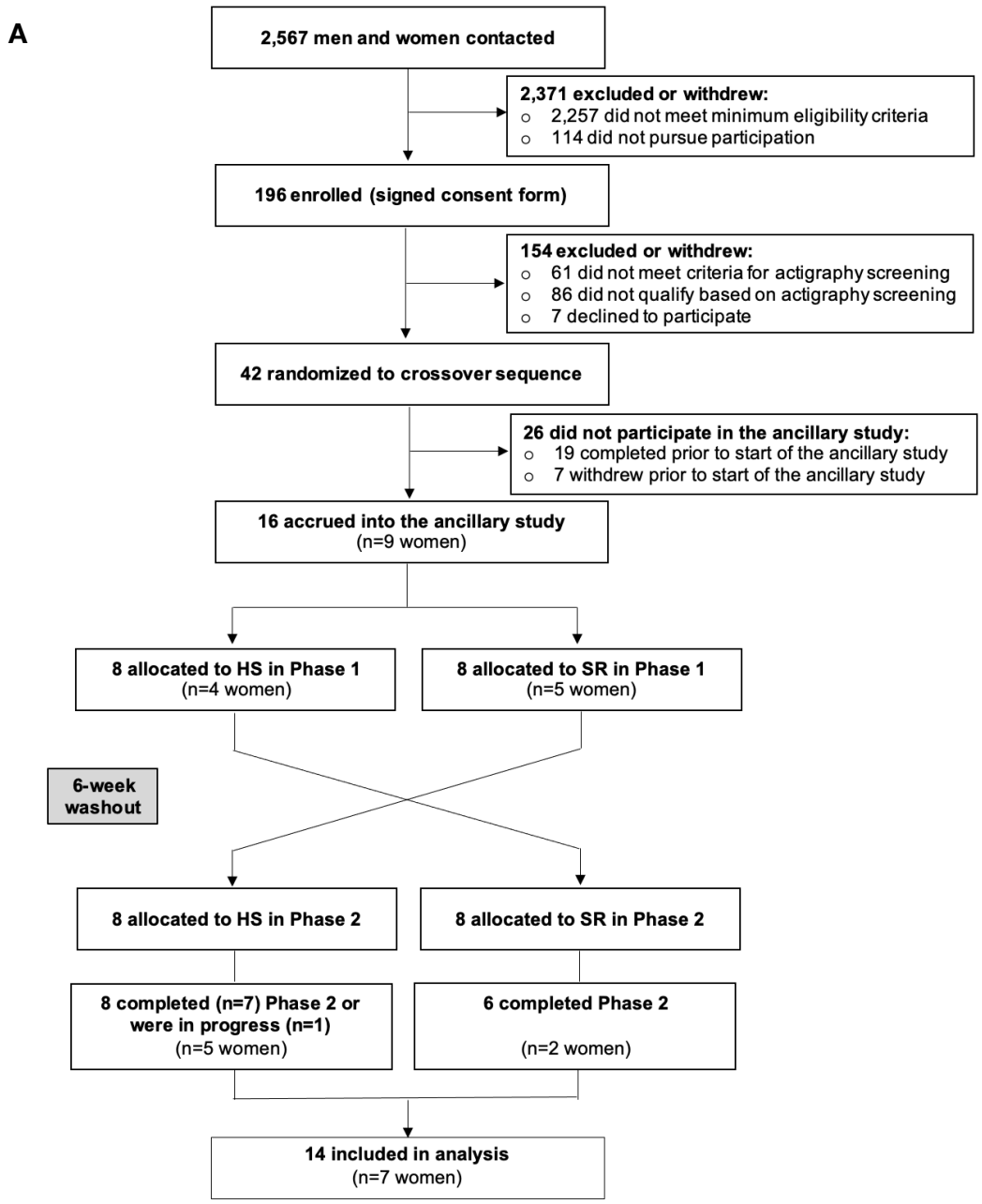
A
2,567 men and women contacted
2,371 excluded or withdrew:
2,257 did not meet minimum eligibility criteria
114 did not pursue participation
196 enrolled (signed consent form)
154 excluded or withdrew:
61 did not meet criteria for actigraphy screening
86 did not qualify based on actigraphy screening
7 declined to participate
42 randomized to crossover sequence
26 did not participate in the ancillary study:
19 completed prior to start of the ancillary study
7 withdrew prior to start of the ancillary study
16 accrued into the ancillary study
(n=9 women)
8 allocated to HS in Phase 1
(n=4 women)
8 allocated to SR in Phase 1
(n=5 women)
6-week washout
8 allocated to HS in Phase 2
8 allocated to SR in Phase 2
8 completed (n=7) Phase 2 or were in progress (n=1)
(n=5 women)
6 completed Phase 2
(n=2 women)
14 included in analysis
(n=7 women)

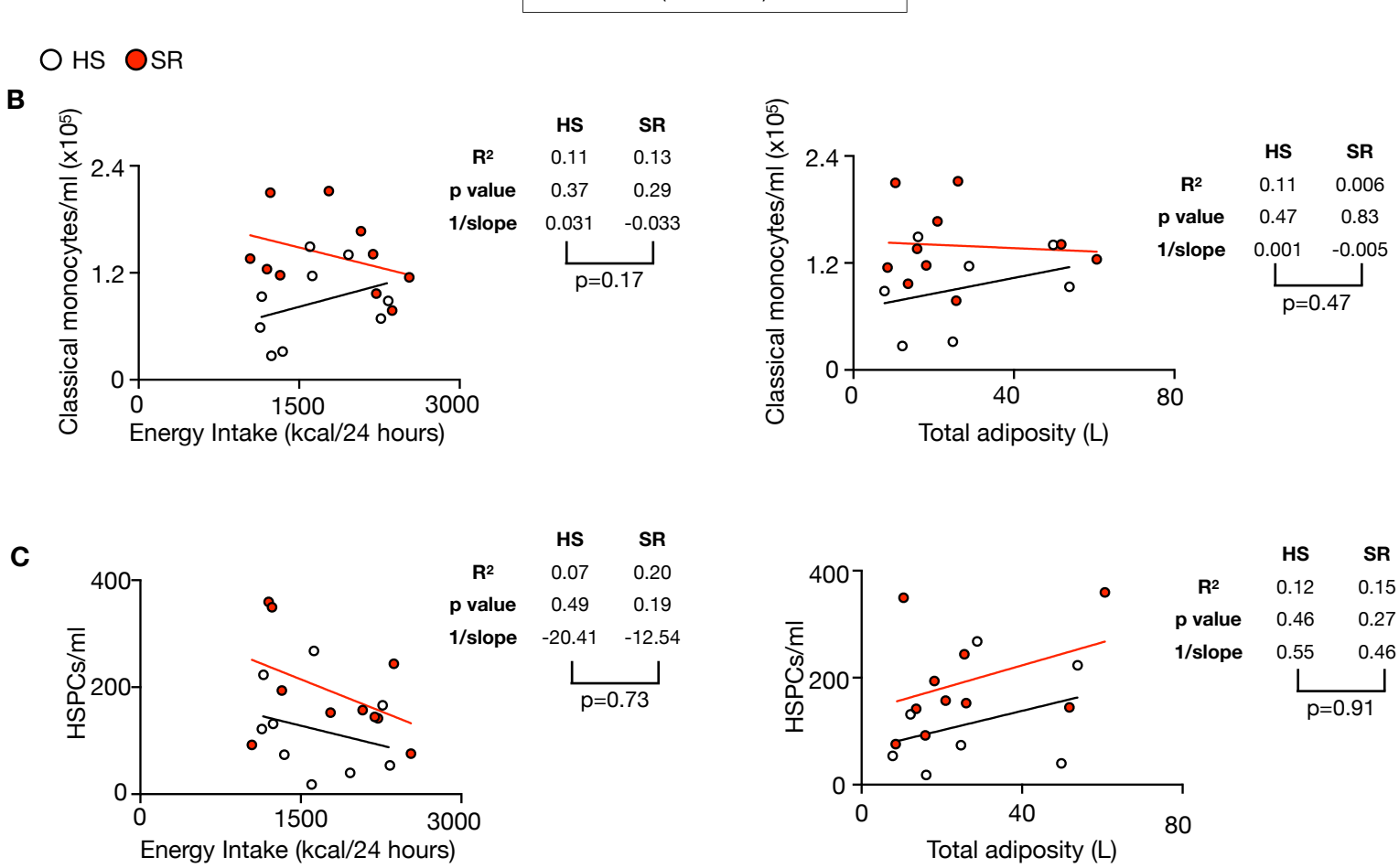
HS SR
B
Classical monocytes/ml (x10⁵)
2.4
1.2
0
0
1500
3000
Energy Intake (kcal/24 hours)
HS SR
R² 0.11 0.13
p value 0.37 0.29
1/slope 0.031 -0.033
p=0.17
Classical monocytes/ml (x10⁵)
2.4
1.2
0
0
40
80
Total adiposity (L)
HS SR
R² 0.11 0.006
p value 0.47 0.83
1/slope 0.001 -0.005
p=0.47
C
HSPCs/ml
400
200
0
0
1500
3000
Energy Intake (kcal/24 hours)
HS SR
R² 0.07 0.20
p value 0.49 0.19
1/slope -20.41 -12.54
p=0.73
HSPCs/ml
400
200
0
0
40
80
Total adiposity (L)
HS SR
R² 0.12 0.15
p value 0.46 0.27
1/slope 0.55 0.46
p=0.91

Figure S5